FINAL REPORT

Grant No. NAG-849-1

PREDICTION OF FORCES AND MOMENTS FOR HYPERSONIC FLIGHT VEHICLE CONTROL EFFECTORS

Mark D. Maughmer
Associate Professor of Aerospace Engineering

Lyle N. Long
Assistant Professor of Aerospace Engineering

Neal Guilmette
Graduate Research Assistant

Peter Pagano
Graduate Research Assistant

Department of Aerospace Engineering
233 Hammond Building
The Pennsylvania State University
University Park, PA 16802
(814) 865-2569

submitted to

National Aeronautics and Space Administration
Langley Research Center
Hampton, Virginia
Attn : David Raney

May 3, 1993

TABLE OF CONTENTS

ABSTRACT

This research project includes three distinct phases. For completeness, all three phases of the work are briefly described in this report. The goal was to develop methods of predicting flight control forces and moments for hypersonic vehicles which could be used in a preliminary design environment.

The first phase included a preliminary assessment of subsonic/supersonic panel methods and hypersonic local flow inclination methods for such predictions. While these findings clearly indicated the usefulness of such methods for conceptual design activities, deficiencies exist in some areas. Thus, a second phase of research was conducted in which a better understanding was sought for the reasons of the successes and failures of the methods considered, particularly for the cases at hypersonic Mach numbers. This second phase involved using computational fluid dynamics methods to examine the flow fields in detail. Through these detailed predictions, the deficiencies in the simple surface inclination methods were determined.

In the third phase of this work, an improvement to the surface inclination methods was developed. This used a novel method for including viscous effects by modifying the geometry to include the viscous/shock layer.

I. INTRODUCTION

Purpose of This Work

In the executive summary of the AGARD Symposium on the Aerodynamic Characteristics of Controls in 1979 [1], it was stated that the need exists for a more extensive and modern data base. Furthermore, it was suggested that additional research be conducted to fill existing gaps in the data base. It was also pointed out that theoretical methods were inadequate in accounting for viscous effects and flow separation. Almost fifteen years later, these comments still apply.

In fact, for hypersonic flight vehicles the situation is actually worse. The data base for hypersonic flight control information is extremely limited. Some available wind-tunnel data is of questionable validity and flight-test results are scarce. Furthermore, in addition to the need to account for viscous effects and flow separation, theoretical prediction methods at hypersonic Mach numbers must also contend with problems involving thin shock layers and real gas effects. Some existing computational fluid dynamic (CFD) methods have the ability to handle such problems, but require too much computer and engineering time to be used routinely for conceptual design studies. Consequently, a real need exists for computationally efficient methods of predicting flight control forces and moments for hypersonic vehicles which provide reasonable results.

The recent push toward the development of hypersonic flight vehicles has highlighted the need for rapid aerodynamic prediction methods [2 - 4]. The complexity of such vehicles demands

the integration of all technological disciplines from the conceptual design stage. Hence, it is of great advantage to be able to analyze many conceptual design proposals and discard those which are not promising. Many methods exist which are capable of performing this analysis; however, at the conceptual design stage monetary and/or time restrictions may preclude their use. CFD techniques are best suited for preliminary or detailed design analysis due to the great length of time required for solution of flows over complex geometries. In addition, the expense and limitations of hypersonic test facilities may relegate their effective use to the testing of final design configurations.

Early integration of control systems into the design process is of paramount importance to the success of a hypersonic vehicle design. At hypersonic Mach numbers, a vehicle traveling through the upper atmosphere will experience dissociation of constituent gases in air. The Space Shuttle Orbiter is a case in point. Upon re-entry, STS-1 required a body flap deflection twice that of the predicted value to trim out the longitudinal moment [5 - 10]. While there is some disagreement over the cause of this problem, most believe it to be due to either real gas effects [11, 12] or low Reynolds number effects [13]. Other complicating features of hypersonic flows are thick boundary layers, entropy layers, thin shock layers, and boundary layer/shock layer interaction, all of which effect the control aerodynamics. Hypersonic vehicles also experience very large center-of-pressure movements as they traverse the flight envelope from low to high speed. Likewise, the design engineer must consider the changes in flap effectiveness due to the flap being embedded in the viscous layer. It is clear from entropy-layer studies [14] that a sharp-nose cone produces a greater pressure recovery on a deflected flap surface than a blunt one. Thus it is concluded that flap effectiveness is decreased by increasing nose bluntness. It is interesting to note that widely used aerodynamic prediction techniques, such as the Aerodynamic Preliminary Analysis System (APAS), other Gentry codes and the Hypersonic Arbitrary Body Program (HABP) make no attempt to account for the effects of the flow field ahead of a control surface. Flap effectiveness is also decreased as the flap deflection angle is increased. This is caused by the viscous layer separating when the flow is deflected far enough relative to the vehicle body. This separation can create a secondary shock system and/or transition the boundary layer, both of which decrease flap effectiveness. It has also been pointed out that there is a need for a substantial data base [14] which must be shared among the various disciplines involved in hypersonic research.

The purpose of this work is to develop and/or improve simple hypersonic aerodynamic methods such as those used in APAS/HABP to better predict viscous and dissociating flow field effects on control surfaces. The initial phase [15] consisted of comparing these simple prediction techniques (data generated using APAS) to experimental data to determine where the greatest need for improvement lies. In this second phase, the flow phenomena (ie. shockwaves, viscosity, chemistry) which have the greatest effect on prediction quality were determined. A secondary goal was to add to the database of hypersonic research by examining a relatively simple geometrical shape (the X-15 airfoil) for a range of Mach number, angle of attack, flap deflection and flow field conditions. In the third and final phase, a new scheme for correcting for viscous effects was developed which is analagous to including the displacement thickness in subsonic methods.

Methodology

Portions of the goals of this research project, as outlined in the preceding section, were attained through the use of an advanced CFD code, the Three-Dimensional Euler/Navier-Stokes Method (TEAM) code (see Section II). This code was essentially used as a hypersonic wind tunnel. CFD is playing a very important role in the advancement of hypersonic technology. Flight testing is a valuable means of collecting data, but it is difficult to accomplish and is often performed post-development. Experimental ground facilities are simply too limited to cover the range of parameters and flight conditions [16]. CFD is not currently the complete solution, there are still many problems to be overcome. It has been suggested, however, that it may provide results as meaningful as those obtained from experimental ground facilities. Such facilities are plagued by the need to extrapolate data to flight conditions, contaminated flow [5], and tunnel peculiar effects on produced data [14]. A major contributor to the tunnel peculiar effects is that of the acoustic environment. The active turbulent boundary layer on the wall of a hypersonic tunnel, as well as any other acoustic disturbances of sufficient strength introduced into the flow-field, will cause transition to occur on the model earlier (at a lower unit Reynolds number) than would be the case for a free-flight experiment [17 - 21].

The lack of experimental hypersonic facilities is yet another impetus for the development and use of CFD codes. A 1968 report to the NASA Subcommittee on Fluid Mechanics of the Committee on Basic Research [22] mentions the need for "wind-tunnel facilities with higher Reynolds number capabilities than are currently available". This is all the more poignant in the 1990's after decades of inactivity in hypersonic research have depleted the number of operational test facilities. The high cost of hypersonic test facilities has often caused their demise. Reference [23] quotes the cost of a Re (based on test section area) = 10 million continuous flow tunnel as over 100 million 1975 dollars.

Thus with an understanding of the shortcomings associated with CFD, and an appreciation of its advantages, a comparison is presented between results from classical Newtonian and tangent wedge theories (both integral components of the APAS/HABP type codes) and results obtained from the TEAM code. Surface pressure plots are compared to illuminate anomalies, and flow-field contour plots from the TEAM code will be shown to explain these differences.

II. THEORETICAL ASPECTS

As discussed in Section I, a comparison is presented between simple hypersonic methods for predicting surface pressure and an advanced CFD technique. The theories pertaining to these various methods is presented here.

TEAM Code

The Three-Dimensional Euler/Navier-Stokes Aerodynamic Method (TEAM) [24] was developed by the Lockheed Aeronautical Systems Company, Burbank, California for the Aeromechanics Division of the Flight Dynamics Laboratory, Wright Research & Development Center under contract of the United States Air Force. The four year (July 1984 - October 1988) effort was the result of a desire to develop a computationally efficient code which could solve both viscous and inviscid flow fields with real-gas effects. Grid system independence was another driving factor in TEAM code development. Grids may be generated using any external program available to the user, only the cartesian coordinates of the grid nodal points are required.

The TEAM code will be briefly described here, a more detailed description is included in the Appendix of this report. TEAM uses a finite-volume spatial-discretization algorithm coupled to a Runge-Kutta time-marching scheme to solve the Navier-Stokes equations. It can use zonal, patched grids and is therefore quite flexible. It also includes implicit residual smoothing, enthalpy damping, and local time-stepping for efficient convergence to a steady state. The code can simulate turbulent, laminar, or inviscid flow of perfect or real gases.

The TEAM code is normally run on a large supercomputer such as a Cray, Convex, or IBM-3090. As a rough rule of thumb, the code requires 25 microseconds/grid point/iteration. Just to illustrate the CPU requirements of this code, some representative cases are illustrated in the following table. This is just an illustration and individual times for particular runs can vary dramatically depending on the flow field and the grid.

Table 1. Estimates of CPU Times for Different Numerical Schemes.

	Inviscid (Euler)		Viscous (Navier-Stokes)	
Dimensions	2-D	3-D	2-D	3-D
No. of Cells	10,000	400,000	20,000	800,000
No. Time Steps	1,000	2,000	10,000	20,000
CPU Time (Cray XMP)	4 Min.	5 Hours	1.4 Hours	111 Hours

This table shows that 3-D, viscous computations are extremely time consuming. It also shows, however, that even a 2-D viscous computation can require hours on a supercomputer. This is one reason for performing the work described herein. In a design environment, one must have tools which are computationally efficient in order to facilitate the iterative nature of design.

Surface Inclination Methods

The nonlinear nature of hypersonic flow manifests itself in such phenomena as high-temperature chemically reacting flow-fields, thin shock layers, entropy layers (vorticity interactions), interactions between the viscous boundary-layer and the shock wave and low-density effects at high altitudes. Considering these phenomena, to obtain a complete picture of the flowfield, one cannot hope to use a simple analytic method. There do exist, however, a number of analytical methods which, under certain circumstances can provide a good first approximation to the coefficients of pressure (and hence to the aerodynamic forces and moments) on a body in a hypersonic inviscid flow-field.

Modified Newtonian Theory

Sir Isaac Newton developed his famous Newtonian flow model more than three centuries ago. It was first published in Propositions 34 and 35 of *Principia* in 1687 [25]. Although developed to explain subsonic flow, this method has seen renewed interest in the latter half of this century as a means of predicting the aerodynamic forces on hypersonic vehicles in the design proposal stage. The equation for this model is obtained by assuming that a flow impacting on a surface looses all momentum normal to the surface, and the flow particles then move tangentially along the surface. Then for a surface inclined at an angle θ to the free-stream,

$$\text{Change in normal velocity} = V_\infty SIN\,\theta$$

$$\text{Mass flux incident on a surface A} = \rho_\infty V_\infty A\, SIN\,\theta$$

$$\text{Time rate of change of momentum of the mass flux} = \rho_\infty V_\infty^2 A\, SIN^2\,\theta$$

Newton's Second Law states that the time rate of change of momentum is equal to the force exerted on a surface. Denoting this force by F,

$$F = \rho_\infty V_\infty^2 A \sin^2\theta$$

Newton assumed the flow of particles to be rectilinear, i.e., no random interaction of fluid particles, such that F is associated only with the linear motion of the particles. Static pressure of a gas is due to the purely random motion of its particles, not accounted for in the Newtonian model. Thus F/A, which has the dimensions of pressure, must be interpreted as the pressure difference above the free-stream static pressure.

$$\frac{F}{A} = p - p_\infty$$

Here p is the surface pressure, and p_∞ is the free-stream static pressure. Combining the previous equations and introducing the pressure coefficient gives

$$C_p = 2\sin^2\theta$$

This result can also be derived from the gas dynamic equations governing oblique shock waves.

Modified Newtonian Theory, as proposed by Lester Lees [26,27], replaces the coefficient of the sine squared term in the previous equation with the coefficient of pressure at the stagnation point behind a normal shock.

$$C_p = C_{p_{max}}\sin^2\theta$$

Where,

$$C_{p_{max}} = \frac{P_{o_2} - P_\infty}{\frac{1}{2}\rho_\infty V_\infty^2}$$

If the dynamic pressure is written as $\frac{1}{2}\rho_\infty V_\infty^2 = \frac{\gamma}{2}p_\infty M_\infty^2$, and use is made of the "Rayleigh Pitot tube formula" [26], then the equation for $C_{p\,max}$ becomes

$$C_{p_{max}} = \frac{2}{\gamma M_\infty^2}\left(\left[\frac{(\gamma+1)^2 M_\infty^2}{4\gamma M_\infty^2 - 2(\gamma-1)}\right]^{\frac{\gamma}{(\gamma-1)}}\left[\frac{1-\gamma+2\gamma M_\infty^2}{\gamma+1}\right]-1\right)$$

It should be noted that in the modified Newtonian theory, C_p is no longer Mach number independent. Further, as the hypersonic limit is approached (as $M_\infty \to \infty$) and $\gamma \to 1$, classical Newtonian theory is recovered. Modified Newtonian theory has been shown to be more accurate than straight Newtonian in the prediction of pressures over blunt bodies.

Tangent Wedge Method

The tangent wedge method was developed to predict the surface coefficient of pressure on two dimensional hypersonic shapes. Suppose it is desired to calculate the pressure at a point *i* on a body. A tangent to the surface is computed at point *i*, making an angle θ_i with the free-

stream. Then the pressure at this point *i* will be determined as if it were on the surface of a two-dimensional wedge of half-angle θ_i, i.e., through the use of exact oblique shock relations. This method assumes that nowhere on the body will the deflection angle to the free-stream be greater than the maximum turning angle for the free-stream mach number. The tangent wedge method has been shown to work best for sharp nosed bodies with attached leading edge shocks.

Hypersonic Shielding

Hypersonic shielding is a method used to treat the leeward side of bodies in hypersonic flowfields. These wake regions are "shielded" from the oncoming free-stream, and because of this, the surface static pressure may be set to zero. Hypersonic shielding is often used, as it is in this research effort, for the shielded part of the body while Newtonian theory or the tangent wedge method is used for the impact side of the body.

The definition of pressure coefficient is

$$C_p = \frac{p - p_\infty}{\frac{1}{2}\rho_\infty U_\infty^2}$$

Thus when $p \rightarrow 0$ (vacuum), this definition gives :

$$C_p = \frac{-p_\infty}{\frac{1}{2}\rho_\infty U_\infty^2}$$

and, since $\frac{p}{\rho} = RT = \frac{c^2}{\gamma}$, the above becomes :

$$C_p = \frac{-2}{\gamma M_\infty^2}$$

which is the pressure coefficient in a vacuum.

III. TEAM CODE VALIDATION

Experimental verification of the numerical results obtained in this research has not been possible due to the limited amount of hypersonic wind-tunnel and flight test data available. Validation of the TEAM code for similar (i.e. hypersonic inviscid and viscous) experiments will therefore be cited as verification of the TEAM code.

<u>Supersonic/Hypersonic Inviscid Cases</u>

The first test case to be discussed involves evaluation of TEAM's ability to model attached and detached shocks in supersonic flows. This was accomplished by running TEAM for both a sharp-nose cone cylinder and a blunt-nose cone cylinder at a Mach number of 2.96 and angles of attack of 0 and 16 degrees using the standard adaptive dissipation scheme. Additionally, the sharp-nose cone cylinder was modeled at Mach number 4.63 for angles of attack of 4 and 24 degrees. Surface pressure data obtained from TEAM is correlated with experimental data from reference [28]. The computational and experimental results are in good agreement except at $\theta = 45°$, where computed surface pressures are below the measured results. The authors of reference [24] cite the absence of viscosity as the most likely cause for the variance.

Additional evaluation of TEAM's ability to predict hypersonic flow-fields is accomplished by trying to duplicate the experimental results of Shindel [29]. A cone-derived hypersonic waverider was tested at Mach = 6 for angles of attack of -4°, the design angle of attack of 0°, and +4°. Computed lift and drag coefficients were in very good agreement with experimental and theoretical values [29]. The data on the upper surface and lower surface correlate well out to about 60% of the semispan. The disagreement beyond this point on the lower surface is primarily due to the absence of a shock/boundary layer interaction model in this region.

A further investigation of hypersonic waverider configurations at off design conditions using the TEAM code has been performed by Long [30]. Inviscid perfect and real gas computations were performed on Rasmussen's elliptical-cone waverider [31]. Computed values of CL, CD and L/D at angle of attack correlate very well with experimental data. Differences between experimental and computational results are attributed to the lack of viscous effects in the computational effort.

Viscous Cases

The first viscous case to be discussed is that of the Lockheed-AFOSR Wing C. This test was conducted at Mach = .85, $\alpha = 5°$ and Re = 10 million based on a mean aerodynamic chord (MAC) of .76 meters. The thin-layer Navier-Stokes (TLNS) approximation to the Reynolds-averaged Navier-Stokes (RANS) equations were solved in the six zones surrounding the wing, and the Euler equations used in the seventh outer zone. Computed surface pressure data are compared with experimental results [32] and an inviscid solution at four stations along the wing. It is evident that the viscous solution better approximates the experimental data. The viscous solution shows a reduction of aft loading and a forward movement of shocks on the wing. It is stated in reference [24] that further research is required to explain the differences between the viscous solution and the experimental data, especially at the outboard stations.

A viscous solution for a double-delta wing-body configuration is another case that was analyzed for the TEAM code validation. This case was run at Mach = .3, $\alpha = 20°$ and R_e = 1 million/ft. The TLNS equations were solved in 12 zones next to the body, the Euler equations used in the remaining four. Turbulent flow was assumed over the entire surface.

Surface pressure data at three cross plane stations for TEAM viscous, TEAM inviscid, and experimental are presented in reference [31]. Better over-all prediction at all stations is evident for the viscous solution. Lift and drag coefficients for the viscous case also better approximate the experimental data [24].

Reference [33] is a viscous investigation of an axisymmetric indented nose cone at Mach = 9.89 intended to compare the results from continuum (Navier-Stokes, Euler) methods with those of a kinetic theory approach (Boltzmann equation). The Navier-Stokes method used is TEAM. The kinetic theory approach is the DSMC (Direct Simulation Monte Carlo) method developed by Bird [34]. Heat transfer predictions for each method are shown to compare very well to experimental data from reference [35]. Other comparisons of surface pressure coefficient, skin friction coefficient, flow-field density and temperature are also made between the two methods without comparison to experimental data. These flow-field correlations are quite good and show at least a good agreement between the methods used in TEAM and a solution of the Boltzmann equation.

IV. PROGRESS

Phase I, Evaluation of Surface Inclination Methods

To help address the need for flight control prediction tools, a research program has been underway specifically to provide methods suitable for conceptual design activities involving aerodynamic flight controls. The initial phase of this research included cataloging existing data for hypersonic vehicles and comparing these data with the results of computationally efficient prediction methods. In particular, a preliminary assessment of the subsonic/supersonic panel methods and the hypersonic Newtonian-flow based methods incorporated in the APAS/HABP code [36,37] has been made. This assessment [15,39,40] includes a comparison of theoretical predictions with results obtained experimentally for the North American X-15, the Hypersonic Research Airplane, and the Space Shuttle. While the experimental data used was taken primarily from wind-tunnel measurements, a few flight-test results for the Shuttle are also included. Comparisons were made from Mach numbers of near zero to twenty.

It was shown that the flow inclination methods do a good job of predicting lift at hypersonic speeds. Most important for flight controls work, the change in lift coefficient due to an elevon deflection is predicted very well. The pitching moment versus angle of attack and control deflection angle for the Shuttle at a Mach number of 5.0, however, is not predicted nearly as well as the lift curve predictions. The change in pitching moment coefficient with control deflection is reasonable, especially at the higher angles of attack. Since separation is not modelled, the results for large control deflections are not good at all. Predicted lateral/directional results (at a Mach number of 5.0) not only agree well with wind-tunnel results, but also agree reasonably well with flight-test data.

This Phase I work has been widely reported. This documentation includes a Masters thesis

[15], a NASP Contractor Report [38], a conference paper [39], and a journal paper [40].

Phase II, Comparisons of Surface Inclination and CFD Methods

After setting up various analysis programs (APAS/HABP, TEAM, and HyperAero) in the early stages of Phase II, efforts turned towards gaining a greater insight into the nature of viscous and real gas effects in hypersonic flows. The main concern of this effort was to discover computationally efficient methods which can accurately predict pitching moments. Toward this end, two-dimensional viscous pressure distributions (excluding real gas effects) have been obtained.

During Phase II, the reasons why the impact methods do not accurately predict some aerodynamic coefficients were explored. The TEAM code was used to accomplish this. This code has been thoroughly tested and can be used as a numerical wind tunnel. It uses a finite-volume, Runge-Kutta algorithm to solve either the Euler equations or the Navier-Stokes equations. It can also model real gas effects and turbulent flow.

Experimental force and moment data are not sufficient to explain the weaknesses of the impact methods, rather, surface pressure data is required. As experimental data such as this is essentially non-existent for hypersonic Mach numbers, advanced CFD techniques were used to generate it.

Initially, the X-15 airfoil was used as a test case. This is a modified NACA 66-005 airfoil. For the purposes of this study, the NACA 66-006 airfoil is scaled down to 5% thickness, since the NACA 66-005 coordinates are not readily available. The oversized leading edge radius and the blunted trailing edge of the actual X-15 were not scaled. The actual coordinates used are shown in Table 2.

At a Mach number of 6.93, angles of attack of 0, 10, and 20 degrees have been considered, with flap deflections of -10, 0, and 10 degrees. At $M=23$, $\alpha = 0$ and 30 degrees with no flap deflections have been considered.

Results for this airfoil have been obtained from both the above described CFD code (in inviscid and viscous mode) and from impact theory. Since this is a two-dimensional problem, instead of using HABP, a simple in-house program was used. This program, called HyperAero, uses the modified Newtonian method, the tangent wedge method, and a vacuum condition for surfaces facing away from the free-stream. The use of these very simple methods is sufficient to allow the determination of what physics must be modelled better in order to more accurately predict the forces and moments.

While the above methods are the simplest approximations possible for hypersonic aerodynamics, their limitations are easily quantified. Thus, a great deal can be learned by comparing modern CFD methods to the above methods. In addition, because HyperAero is

Table 2. Modified NACA 66-006 Coordinates

X	Y Upper	Y Lower
0.00000	0.00000	0.00000
0.00003	0.00039	-0.00039
0.00007	0.00058	-0.00058
0.00013	0.00076	-0.00076
0.00020	0.00095	-0.00095
0.00029	0.00112	-0.00112
0.00040	0.00129	-0.00129
0.00052	0.00144	-0.00144
0.00065	0.00159	-0.00159
0.00079	0.00172	-0.00172
0.00095	0.00185	-0.00185
0.00111	0.00198	-0.00198
0.00128	0.00210	-0.00210
0.00500	0.00376	-0.00376
0.00750	0.00449	-0.00449
0.01250	0.00563	-0.00563
0.02500	0.00769	-0.00769
0.05000	0.01058	-0.01058
0.07500	0.01279	-0.01279
0.10000	0.01465	-0.01465
0.15000	0.01765	-0.01765
0.20000	0.01997	-0.01997
0.25000	0.02177	-0.02177
0.30000	0.02312	-0.02312
0.35000	0.02408	-0.02408
0.40000	0.02468	-0.02468
0.45000	0.02493	-0.02493
0.50000	0.02481	-0.02481
0.55000	0.02424	-0.02424
0.60000	0.02315	-0.02315
0.64999	0.02144	-0.02144
0.70000	0.01912	-0.01912
0.75000	0.01622	-0.01622
0.80000	0.01286	-0.01286
0.85000	0.00921	-0.00921
0.90000	0.00553	-0.00553
0.95000	0.00222	-0.00222
1.00000	0.00000	0.00000

a Fortran program that is only about 150 lines long, modifications and numerical experiments can be performed very easily. Once it is understood how to obtain accurate predictions for control surface deflections, these will be incorporated into APAS/HABP.

Inviscid CFD Predictions

This section describes the inviscid CFD results and compares them to surface inclination predictions. The grid used in the (inviscid) TEAM code is shown in Figure 1 and had 6,144 cells. Several grid sensitivity studies were conducted to determine how fine to make the grid. The grid used is extremely fine and should result in accuracies that are within a few percent. Figures 2a - 12a show surface pressure predictions (from HyperAero and inviscid TEAM) for the Mach = 6.83 cases. Figures 2b - 12b show the TEAM code flow fields shaded according to pressure for the Mach = 6.83 inviscid cases. The shading actually corresponds to the natural logarithm of the pressure in order to show the gradients better. Since HyperAero predicts only surface quantities (not the whole flow field), the TEAM and HyperAero flow fields cannot be compared directly.
Figures 2a, 3a, and 4a show the surface pressure predictions from TEAM, tangent wedge, and Newtonian flow for α = 0 degrees and δ = -10, 0, and + 10 degrees, respectively, where α is the angle of attack and δ is the flap deflection angle. The Euler code solution is quite smooth, but the HyperAero solution shows a rapid change in the pressure coefficient, C_p, at the mid-chord. This is due to the sudden change from the tangent wedge method to the vacuum method. In the tangent wedge method $C_p = 0$; however, as soon as $\theta \leq 0$ the method gives the vacuum value for C_p. It is interesting to note that the Euler code produces a smooth result that is approximated by the HyperAero code. It should also be noted that the Euler code predictions are very close to vacuum conditions on the upper surface near the trailing edge, such that HyperAero and TEAM agree quite well there. Also, the HyperAero method agrees well with TEAM on the upper surface of the flap since the flow is approximated quite well by a vacuum in that region. Although the tangent wedge method agrees reasonably well with TEAM near the leading edge, predictions on the lower surface of the flap do not agree well with TEAM. This severely effects the moment prediction.

The impact methods are known to predict the flow field at low angles of attack poorly. In fact, Hankey [41] claims that more refined methods must be used for angles of attack below 10 degrees. He also says that "only gliders having L/D's greater than 4 will fly at angles of attack less than 10 degrees." Thus, at low angles of attack one can expect problems in using impact methods.

Figure 5a shows the results of the three prediction methods (inviscid TEAM, tangent wedge, and Newtonian) for α = 10 and δ = 0 degrees. In this case, the tangent wedge method agrees better with TEAM than the Newtonian method, which is what one would expect. Typically, tangent wedge works better for flat surfaces at large angles of attack, while Newtonian will work better on blunt bodies or stagnation regions. Even though the tangent wedge method

predicts the surface pressure very well over most of the airfoil, however, differences are observed between the TEAM code and tangent wedge at the leading and trailing edges. This immediately indicates a possible error in the moment prediction. The leading edge discrepancy is due to the transition from tangent wedge (or Newtonian) to the vacuum method. The flow transitions from compression to expansion very near the leading edge, but the jump from Newtonian to vacuum is not as noticeable at $\alpha = 10$ degrees as it was at $\alpha = 0$ degrees. While the TEAM code gradually expands the flow around the corner, the transition with the impact methods is quite abrupt.

In Figure 6a the results for $\alpha = 10$ degrees and $\delta = 10$ degrees are shown. While tangent wedge clearly agrees better with TEAM over most of the airfoil, the Newtonian method once again agrees better over the flap surface. In Figure 7a, the results for $\alpha = 10$ degrees and $\delta = -10$ degrees are shown. In this case, the flap is aligned with the flow direction, but the airfoil is at an angle of attack. Since the impact methods do not account for any upstream influences, the flap does not "know" the airfoil is at $\alpha = 10$ degrees. Consequently, the tangent wedge and Newtonian methods both predict the same C_p's on the flap that they predict for $\alpha = 0$ degrees and $\delta = 0$ degrees. The TEAM code flow field, however, has already been turned by the airfoil and must re-expand (lower surface) or re-compress (upper surface) the flow. This discrepancy in the impact methods may cause a significant error in the moment and, possibly, even in the lift.

Figure 8a shows the results for $\alpha = 20$ degrees and $\delta = 0$ degrees. At these higher angles of attack, the impact methods become quite effective and the tangent wedge method clearly agrees better with TEAM than the Newtonian method. Some discrepancies remain at the leading edge, however, due to the rapid transition from tangent wedge to vacuum method. There are also inconsistencies at the trailing edge.

Figure 9a and 10a show the surface pressure predictions for $\alpha = 20$ degrees and $\delta = 10$ degrees and $\delta = -10$ degrees, respectively. For $\delta = 10$, neither the Newtonian or tangent wedge method agree with TEAM on the flap. This case results in very strong shockwaves, one starting at the leading edge and the other starting at the flap leading edge. These are clearly visible in the flow field shown in Figure 9b. It is important to investigate viscous results for this case, since significant shock/boundary layer interactions probably exist. The Euler results cannot be assumed correct for this case. For the negative flap deflection (Figure 10a), the tangent wedge method does a fairly good job predicting the inviscid TEAM code results.

Figures 11 and 12 show predictions for Mach = 23. At $\alpha = 0$ degrees, the methods all agree fairly well except at the leading edge. At $\alpha = 30$ degrees, the shockwave is extremely strong and both Newtonian and tangent wedge results deviate from those of the TEAM code. It would be useful to evaluate real gas effects at this Mach number.

In all the flow field images, one can clearly see the shock wave starting at the leading edge.

For a point source travelling at Mach = 6.83, one would expect a Mach cone angle of

$$\beta = \frac{1}{M} = \frac{1}{6.83} = 0.145 \text{ radians} = 8.4 \text{ degrees}$$

This is roughly the shock angle near the nose shown in Figure 2b (α =0 degrees). If the airfoil under consideration were a flat plate, the relation between the shock angle, β, and the angle of attack, α, would be governed by

$$\frac{\beta}{\alpha} = \frac{\gamma+1}{4} + \sqrt{\frac{(\gamma+1)^2}{4} + \frac{1}{M^2\,\alpha^2}}$$

Thus, for α = 10 degrees, Mach number = 6.83, and the ratio of specific heats, γ = 1.4,

$$\beta = 16.3 \textit{ degrees}$$

and the angle between the airfoil and the shock would be 6.3 degrees. This is roughly what is observed in Figure 5b. The Newtonian flow method assumes the shock wave lies directly on the body surface, which is only true for infinite Mach number and γ = 1.0.

The surface pressure plots and flow field images presented in this section provide an enormous amount of data. From the above discussion one can see how readily the source of the errors in the impact methods can be determined. During Phase I of this research, numerous problems were uncovered with the use of the impact methods, but force and moment data alone does not provide enough information to determine what causes the problem or to propose corrections to the impact methods or their usage.

The force and moment predictions for the preceding cases are summarized in Table 3. While, it is often difficult to digest large tables of numerical data, it is included for completeness. These data illustrate how well the force and moment data can agree, even though the surface pressure may be quite different. They also show how, in other cases, the different prediction methods can disagree by a large margin.

One must be careful in interpreting the results presented here. Only inviscid (i.e. Euler equation) TEAM code results have been presented in this section. One cannot assume that these are completely correct. In some of the cases presented, viscous effects may be quite significant. These will be presented in the next section. While it is quite legitimate to compare inviscid methods to tangent wedge, Newtonian, and vacuum techniques, since they can all be derived from inviscid gas dynamics, methods such as modified Newtonian have some empiricism built into them. Thus, while it will be strictly fortuitous when methods based solely on inviscid techniques agree with viscous results, the empirically based methods may be expected to predict some viscous behavior since they have been "tuned" to yield correct results.

Table 3. Forces and Moment Predictions

Method	α (Deg.)	δ (Deg.)	CL	CD	CM
Newtonian	0	0	0.0000	0.0092	-0.0000
Tang. Wdg.	0	0	0.0000	0.0114	-0.0000
TEAM Inv.	0	0	0.0000	0.0110	-0.0000
Newtonian	0	+10	0.0106	0.0103	-0.0096
Tang. Wdg.	0	+10	0.0229	0.0140	-0.0207
TEAM Inv.	0	+10	0.0074	0.0122	-0.0069
Newtonian	0	-10	-0.0106	0.0104	0.0096
Tang. Wdg.	0	-10	-0.0229	0.0140	-0.0207
TEAM Inv.	0	-10	-0.0074	0.0121	0.0069
Newtonian	10	0	0.088	0.0248	-0.0346
Tang. Wdg.	10	0	0.160	0.0037	-0.0686
TEAM Inv.	10	0	0.121	0.0331	-0.0502
Newtonian	10	+10	0.111	0.0335	-0.057
Tang. Wdg.	10	+10	0.189	0.0507	-0.097
TEAM Inv.	10	+10	0.141	0.416	-0.069
Newtonian	10	-10	0.077	0.0236	-0.0251
Tang. Wdg.	10	-10	0.137	0.0353	-0.0480
TEAM Inv.	10	-10	0.111	0.0310	-.0407
Newtonian	20	0	0.231	0.0948	-0.105
Tang. Wdg.	20	0	0.331	0.1312	-0.156
TEAM Inv.	20	0	0.315	0.1282	-0.145
Newtonian	20	+10	0.267	0.1198	-0.144
Tang. Wdg.	20	+10	0.371	0.1616	-0.200
TEAM Inv.	20	+10	0.356	0.1578	-0.190
Newtonian	20	-10	0.208	0.0863	-0.083
Tang. Wdg.	20	-10	0.303	0.1187	-0.128
TEAM Inv.	20	-10	0.292	0.1170	-0.122

Viscous CFD Predictions

The TEAM code has also been used to compute the viscous flow fields of 2-D airfoil sections [42]. Viscous pressure distributions have been obtained for three angle of attack/flap deflection combinations ($\alpha = 0°/\delta = 10°$, $\alpha = 10°/\delta = 0°$, and $\alpha = 10°/\delta = 10°$) for the NACA 66-005 airfoil (as used on the North American X-15) at a free stream Mach number of 6.83 and a Reynolds number of 3.3×10^6. The viscous grid is shown in Figure 13. The viscous results have been compared to inviscid TEAM results in Figures 14, 15, and 16, respectively. It can be seen that viscosity drastically alters the pressure distribution on the section surface. As expected, these results indicate that viscosity greatly reduces the effectiveness of the control surface (a twenty-percent-chord flap). Furthermore, the results demonstrate that the presence of viscosity tends to shift the pressure distribution toward greater suction (except for the surface of the deflected flap). It can be seen that these viscous affects would yield sectional lift coefficients similar to those of the inviscid cases; however, they may result in pitching moment differences.

Figures 17, 18, and 19 are the viscous flowfield pressure contours for the three cases, $\alpha = 0°/\delta = 10°$, $\alpha = 10°/\delta = 0°$, and $\alpha = 10°/\delta = 10°$, respectively. By comparing the viscous and inviscid flowfields (Figures 3b, 5b, and 6b), it can be seen that viscosity tends to reduce the flowfield pressures everywhere, except in the vicinity of a deflected control surface. (As is consistent with results given in Figures 14 through 16.)

Table 4 summarizes the force and moment predictions using four methods of analysis: modified-Newtonian, tangent-wedge, TEAM Euler, and TEAM Navier-Stokes. It should be noted that the Navier-Stokes and Euler analyses yield very similar force and moment coefficients for all three test cases. These results suggest that viscosity has little effect at these conditions. Table 4 also yields information by which the local surface inclination methods (modified-Newtonian and tangent-wedge) may be assessed. By comparing these two methods to the viscous TEAM results, some interesting trends may be seen. First, since both inclination methods overpredict the lift and moment coefficients at zero angle of attack, it is clear that these methods also greatly overpredict control surface effectiveness. Secondly, for all three test cases, the viscous drag coefficients consistently fall in between those predicted by tangent-wedge and modified-Newtonian. In all cases, modified-Newtonian underpredicts the magnitude of the viscous drag coefficient and tangent wedge overpredicts these magnitudes. This trend also holds for the lift and moment coefficients of both $\alpha = 10°$ cases. To more fully understand these effects, it is beneficial to investigate the pressure distributions predicted by these methods.

Figures 20, 21, and 22 compare the three viscous TEAM results to pressure predictions from tangent wedge and Newtonian flow methods. These plots indicate that the viscous pressure distributions are most closely predicted by Newtonian flow over the flap and by tangent wedge over the main element; however, improvements in these approximations for force and moment predictions would be beneficial. Furthermore, these results indicate that the use of hypersonic

shielding does not satisfactorily predict the viscous pressure distribution on leeward surfaces. A more complete description of the results of this section can be found in Reference [42].

Phase III, Improvements to Surface Inclination Methods

Because of the deficiencies of the simple local surface inclination methods (modified-Newtonian and tangent-wedge) in accurately predicting the pressure distribution over an entire airfoil, an improvement to these methods is desired. To investigate this, an inverse approach to the simple analysis methods has been implemented [43]. A first attempt toward this end was an inversion of the modified-Newtonian law. Since the pressure distribution is known from TEAM results and C_{pmax} may be calculated using the "Rayleigh Pitot tube formula", modified-Newtonian can be used to solve for the local surface inclination angle, δ. This is explicitly represented as:

$$\theta = \sin^{-1}\sqrt{\frac{C_p}{C_{p_{max}}}}$$

Using this equation, the local inclinations and, subsequently, a surface that will result in the "correct" (TEAM) pressure distribution when analyzed using modified-Newtonian can be found. In essence, the airfoil geometry is altered such that the TEAM results are achieved. Such an inversion of modified-Newtonian is meaningful only for positive pressure coefficients, since negative C_p's result in imaginary arguments of the arcsine. Also it should be noted that the local inclination, θ, may be positive or negative in sign. Positive inclinations on the airfoil upper surface and negative inclinations on the lower surface gives the proper results.

Using the described inversion of the modified-Newtonian method, surfaces have been determined for each of the three viscous TEAM results. The results of these calculations are shown in Figures 23 - 25. Each plot shows the surface calculated by the inverse analysis, as well as the original X-15 airfoil, at an angle of attack. Analyzing these surfaces using modified-Newtonian produces the viscous TEAM results. Thus, these surfaces capture all of the viscous effects of shock layers, entropy layers and viscous interaction. Since these surfaces are essentially merged shock layers attached at the airfoil leading edge, they will be referred to simply as 'shock layers' hereafter.

Of most interest is the plot of the shock layer thickness (normal to the airfoil chordline) as a function of the chordwise position. Figures 26 and 27 show the lower and upper shock layer thicknesses, respectively, for all three TEAM results. These plots reveal an interesting result: for the flight conditions shown, the shock-layer thickness is nearly a linear as a function of chordwise position up to the control surface. At the control surface, the flap deflection is 'subtracted' from the lower shock layer and 'added' to the upper shock layer. It should also be noted that the two $\alpha = 10°$ shock layer thicknesses are nearly identical (for both the lower and upper surfaces) upwind of the flap. This shows close agreement with the principle that, for supersonic flows, downstream perturbances (i.e., the flap) have no effect on upstream flow characteristics. One could speculate that the small differences in these curves could be due to shock and viscous interactions within the subsonic portion of the viscous layers, however,

additional investigations are necessary to arrive at any conclusions in this regard. These plots also suggest that higher angles of attack tend to make the shock layer thicker on the upper surface and thinner on the lower surface, as one would expect.

These results indicate that the addition of a linear shock layer thickness to the original airfoil coordinates may result in reasonably accurate viscous pressure distributions when analyzed using modified-Newtonian theory. Should this be the case for various hypersonic flight conditions, this would provide a useful, computationally efficient method for predicting 2-D pressure distributions. Further investigation is necessary, however, in order to attempt to correlate the variance of the shock-layer thickness curve slope to various parameters. These parameters could include Mach number, Reynolds number, the ratio of specific heats, γ, angle of attack, flap deflection, airfoil thickness, and relative size of the control surface. In addition, limitations of such a methodology must be addressed as well. For example, this geometry modification may be limited to low Mach numbers and small angles of attack, or perhaps there may be a requirement of attached shocks.

In addition to correlating the parameters to sectional (2-D) results using modified-Newtonian and/or tangent wedge, future work will include attempting to incorporate a similar shock-layer into 3-D analyses in the hopes of more accurately predicting total aircraft forces and pitching moments due to control deflections.

Table 4: Force and Moment Predictions using Modified Newtonian (MN), Tangent Wedge (TW), TEAM Euler (E), and TEAM Navier-Stokes (NS).

Method	α (deg.)	δ (deg.)	C_L	C_D	C_M
MN	0	10	0.0106	0.0104	-0.0096
TW	0	10	0.0229	0.0140	-0.0207
E	0	10	0.0074	0.0122	-0.0069
NS	0	10	0.0066	0.0134	-0.0055
MN	10	0	0.088	0.0248	-0.035
TW	10	0	0.160	0.0378	-0.069
E	10	0	0.122	0.0331	-0.050
NS	10	0	0.123	0.0347	-0.051
MN	10	10	0.111	0.0335	-0.057
TW	10	10	0.190	0.0507	-0.097
E	10	10	0.141	0.0416	-0.069
NS	10	10	0.140	0.0428	-0.068

V. SUMMARY

In summary, a CFD database has been generated which can be used in the development of a simple method for he prediction of flight control forces and moments. Significant improvements are possible in the existing flow inclination methods.

In addition, this database has been used in an inverse sense to determine the amount of "shock layer" that must be added to the original body in order that the Newtonian method produces pressure distributions in agreement with Navier-Stokes predictions. This method is quite easy to implement because the shock layer that must be added is linear.

APPENDIX: TEAM Code Description

The Three-Dimensional Euler/Navier-Stokes Aerodynamic Method (TEAM) [24] was developed by the Lockheed Aeronautical Systems Company, Burbank, California for the Aeromechanics Division of the Flight Dynamics Laboratory, Wright Research & Development Center under contract of the United States Air Force. The four year (July 1984 - October 1988) effort is the result of a desire to develop a computationally efficient code which could solve both viscous and inviscid flow fields with real-gas effects. Grid system independence was another driving factor in TEAM code development. Grids may be generated using any external program available to the user, only the cartesian coordinates of the grid nodal points are required. Furthermore, a grid may be subdivided into multiple zones, each zone having its own topology, as well each zone may be specified for solution by a different method, ie. "zone 1" may be solved using the Reynolds averaged Navier-Stokes equations, and "zone 2" by using the Euler equations, etc. Zones are specified and "patched" together with a boundary condition data file which is read by TEAM at execution.

The Reynolds averaged Navier-Stokes equations (RANS) are the widely used mathematical models for the flow of a turbulent gas in thermodynamic equilibrium. These are the equations for conservation of mass, linear momentum and energy which have been time averaged. In integral form,

$$\frac{\partial}{\partial t}\int_{\Omega} \vec{w}\, d\Omega + \int_{A} \vec{F}^{c}\, dA = \frac{\sqrt{\gamma} M_{\infty}}{Re_{\infty}} \int_{A} \vec{F}^{v} dA.$$

where $\vec{w}$ is the vector of non-dimensionalized dependant variables

$$\vec{w} = \begin{pmatrix} \rho \\ \rho u_i \\ \rho E \end{pmatrix}$$

F^c and F^v are the convective and viscous flux vectors given by,

$$\vec{F}^{c} = \begin{pmatrix} \rho u_n \\ \rho u_i u_n + P\, n_i \\ \rho H u_n \end{pmatrix}$$

$$\vec{F}^{v} = \begin{pmatrix} 0 \\ \tau_{ij}\, n_j \\ \tau_{jk} u_k n_j - q_n \end{pmatrix}$$

Here ρ is the mass density, u_i are the three cartesian velocity components, E is the total energy, $\hat{n}$ denotes a unit normal vector to the surface, q_∞ is the non-dimensional free-stream speed and Re_∞ is the free-stream Reynolds number based on a characteristic length. A subscript n means the dot product with the vector **n** has been taken. Standard summation notation is employed with the subscripts i (or j or k) = 1, 2, and 3, which correspond to the cartesian coordinates X,

Y, and Z, respectively. $H = E + \frac{P}{\rho}$ is the total enthalpy, and P is the static pressure. For Newtonian fluids, the viscous stress tensor, τ_{ij}, and heat flux, q_j, are related to the mean flow quantities by,

$$\tau_{ij} = \mu_e\left(\frac{\partial u_i}{\partial x_j} + \frac{\partial u_j}{\partial x_i}\right) + \lambda_e\frac{\partial u_k}{\partial x_k}\delta_{ij}$$

$$q_j = -\left(\frac{\gamma}{(\gamma-1)Pr}\right)k_e\frac{\partial T}{\partial x_j}$$

where T is the static temperature, Pr is the free-stream molecular Prandtl number, γ is the ratio of specific heats, μ_e and k_e are the effective dynamic viscosity and thermal conductivity respectively, each is the sum of a molecular and a turbulent part. The effective secondary viscosity, λ_e, is defined by Stokes' hypothesis to be $-2\mu_e/3$. Stokes' hypothesis is most accurate for a monatomic gas, and is a reasonable approximation for incompressible air; however, it's use in compressible applications is suspect. The viscous stress tensor is assumed to be symmetric, and all variables are non-dimensional, see section 3.1 [24].

For a large range of flight conditions, air may be assumed to be a perfect gas. This model condition of rigid rotating diatomic molecules may be represented by fixing $\gamma = 1.4$, estimating static pressure from the equation of state,

$$P = (\gamma - 1)\rho\left(E - \frac{1}{2}u_j u_j + H_\infty\right)$$

Sutherland's law is used to estimate the molecular dynamic coefficient of viscosity.

$$\mu = T^{\frac{2}{3}}\left(\frac{1 + \frac{110.4}{\bar{T}_\infty}}{T + \frac{110.4}{\bar{T}_\infty}}\right)$$

Here $\bar{T}_\infty$ is the dimensional free-stream temperature, $T = P/\rho$, and thermal conductivity is estimated as $k = T^{0.71}$.

Equilibrium real gas calculations, which become important for the determination of body surface temperature and density at high mach numbers are an option available to the user of TEAM [17, 44]. These calculations are performed using curve fits developed by Srinivasan et al. [45,46]. The user must specify free-stream static pressure and density, which are used to estimate free-stream temperature, and free-stream specific enthalpy and specific energy, the ratio of which define γ. Values for local static pressure, temperature, speed of sound, viscosity coefficient and thermal conductivity are then determined from the aforementioned curve fits using the estimated values of local specific energy and density.

For viscous computations, the turbulence model used in TEAM is the well known Baldwin-

Lomax Turbulence Model (BLTM) [47], or one can use laminar flow. Inviscid computations are carried out by solving the Euler equations. These will not be written explicitly here as they are derived by simply setting the viscous terms equal to zero. The Euler equations may be solved with either perfect or real gas computation models as previously described.

Numerical dissipation needs to be included in the TEAM code primarily for two reasons, 1) stability of the solution process and 2) shock capturing [24]. Stability must be numerically enhanced, as inviscid or high Reynolds number calculations have little or no physical dissipative phenomena. Without this artificial dissipation, the solution may become "saw-toothed" with alternating signs at neighboring cells. Often solutions of the RANS equations also require numerical dissipation when the physical (viscous) dissipation is not adequate.

Shock capturing is performed automatically when solving the RANS equations. Euler solutions, on the other hand, do not contain the means to enforce an entropy condition as required by the second law of thermodynamics, hence providing a solution which is not physically realistic. The addition of dissipative terms which imitate the physics inside a shock wave circumvents this error. TEAM provides a choice of three adaptive and two characteristic based dissipation schemes. As this is a study in hypersonics, a characteristic-based scheme is employed. An upwind second order (USO) accurate scheme known as the symmetric TVD formulation [48,49] allows for the capturing of strong shocks encountered at hypersonic speeds. The price of this improved shock capturing is an increase in the number of arithmetic operations, as compared to adaptive schemes. It is also not possible to satisfy the condition of constant total enthalpy for a steady state Euler solution, which is precipitated by the inconsistency of the steady-state mass and energy conservation equations each of whose dissipative terms are constructed independently.

TEAM requires the user to specify a boundary condition at all grid edges and interfaces. This specification then allows the code to create "ghost cells" beyond the grid boundaries and assign a value of the dependant variable in the image cell which, when the fluxes of the cells (boundary and image) are averaged, gives the proper boundary condition dependant evaluation of the flux vector at the cell face.

Far-field boundary conditions are specified at boundaries where the flow is incoming or outgoing. Hypersonic/supersonic flow dictates that all of the flow quantities in the image cells at inflow boundaries be set to their free-stream values. At the outflow boundary, all image cell quantities are set to their boundary cell values. These criteria are determined by the direction of the characteristics at the corresponding boundaries.

Solid surface boundary conditions are prescribed differently for the Euler equations as compared to the Navier-Stokes equations. Inviscid flow requires the no-normal-flow condition be satisfied at solid boundaries. TEAM provides a choice of three methods to satisfy this condition. That used for this research is the simplest and most robust of the three. Surface pressure is set equal to the cell-center value, this pressure on the cell face is the only variable to contribute to the momentum flux balance. The convective flux may be set to zero at the cell

face to preserve the no-normal-flow condition. A surface boundary condition for solution of the RANS equations is the no-slip condition. This condition is imposed by setting the image-cell values of the cartesian components of momentum to be negative of the boundary-cell values, thus insuring the momentum be zero at the surface. The same method of estimating surface pressure as in the inviscid cases was employed for viscous runs. Surface temperature may be prescribed, or an adiabatic condition imposed. In the case of the latter, a zero normal temperature gradient is imposed on the surface to estimate the value of the image-cell temperature.

Grid branch cuts must be specified as "fluid" conditions in the boundary condition dataset. Values for the image-cells on one side of the branch cut are set to those of the boundary-cells across the branch cut, for both sides of the branch cut.

Boundary conditions for planes of symmetry are specified by mirroring the flow field across the plane, eg. across an X-Z plane of symmetry, the Y-component of momentum changes sign while all other variables remain the same as their boundary-cell counterparts. For the 2-dimensional cases used in this research effort, two planes of symmetry were specified with one cell between them.

The semi-discrete approximation which is to be integrated in time is as follows.

$$\frac{d}{dt}(\Omega w) + Q^c - Q^v - D = 0$$

Here Q^c is the convective flux, Q^v is the viscous flux, D is the dissipation and Ω represents the volume. Since the volume Ω is independent of time this equation may be rewritten as,

$$\frac{dw}{dt} + R(w) = 0$$

where R is the residual defined as,

$$R(w) = \frac{1}{\Omega}(Q^c(w) - Q^v(w) - D(w))$$

Thus is defined a system of ordinary differential equations which may be solved by a variety of time marching schemes. Time accuracy is not important here as a computationally efficient steady state solution is the goal. TEAM uses an explicit multistage time-stepping scheme. This scheme allows relatively large time-steps and is easily vectorizable to exploit the capabilities of modern supercomputers. This m-stage hybrid scheme can be represented as follows.

$$
\begin{aligned}
w^{(0)} &= w^{n} \\
w^{(1)} &= w^{(0)} - \alpha_1 \Delta t^* R^{(0)} \\
w^{(2)} &= w^{(0)} - \alpha_2 \Delta t^* R^{(1)} \\
&\vdots \\
w^{(m-1)} &= w^{(0)} - \alpha_{m-1} \Delta t^* R^{(m-2)} \\
w^{(m)} &= w^{(0)} - \alpha_m \Delta t^* R^{(m-1)} \\
w^{n+1} &= w^{(m)}
\end{aligned}
$$

Where $\Delta t^* = CFL \cdot \Delta t$, the Courant number, CFL is a user specified parameter which scales the time step Δt. A pseudo time stepping, or spatially varying time step substantially reduces the number of time steps to convergence. This involves using a local time step for each cell, rather than a globally minimum time step. One consequence of pseudo time stepping is that the solution is no longer time accurate, ie. the solution is meaningless until convergence is reached. Viscous computations often require a much smaller time step than inviscid calculations because they require finer, highly clustered grids. TEAM allows the user to choose between three options for selecting the time step. 1) An inviscid time step in conjunction with two evaluations of numerical and viscous dissipation, 2) application of the modified Crocco's scheme to scale the inviscid time step to satisfy a viscous stability limit, 3) use of a formulation proposed by Tannehill et al. [50], which estimates the time step to automatically satisfy the viscous stability criteria. In this research project, method 1) for inviscid calculations, and method 3) for viscous calculations has been used.

Aerodynamic forces and moments on a body are determined by integrating the normal and tangential stresses. Shear stresses are, of course, absent for an inviscid computation. Denoting normal forces by superscript N, and shear forces by superscript S, force vectors and force coefficients in the body-fixed coordinate system are as follows.

$$\vec{F} = \vec{F}^N + \vec{F}^S \quad and \quad \vec{C}_F = \vec{C}_F^N + \vec{C}_F^S$$

$$\vec{F}^N = \int_{A_s} p\,\hat{n}\,dA \quad and \quad \vec{C}_F^N = -\frac{2}{A_{RA_s}} \int C_p\,\hat{n}\,dA$$

$$\vec{F}^S = -\int_{A_s} \vec{\tau}\,dA \quad and \quad \vec{C}_F^S = -\frac{2}{\gamma M_\infty^2 A_{RA_s}} \int \vec{\tau}\,dA$$

Here p is static pressure, and $\vec{\tau}$ is the dot product of the stress tensor and the unit normal vector $\hat{n}$.

The moments and moment coefficients about a point with position vector $\vec{r}$ are given by:

$$\vec{M} = \vec{M}^N + \vec{M}^S \quad and \quad \vec{C}_M = \vec{C}_M^N + \vec{C}_M^S$$

$$\vec{M}^N = -\int_{A_s} p\,(\vec{r} \times \hat{n})dA \quad and \quad \vec{C}_M^N = -\frac{2}{A_R c_R A_s}\int C_p\,(\vec{r} \times \hat{n})dA$$

$$\vec{M}^S = -\int_{A_s} \vec{r} \times \vec{\tau}\,dA \quad and \quad \vec{C}_M^S = -\frac{2}{\gamma M_\infty^2 A_R c_R A_s}\int \vec{r} \times \vec{\tau}\,dA$$

Here A_R is the reference area, and c_R denotes the reference chord used in defining the force and moment coefficients. Coefficients of lift, drag and side-force, and the coefficients of the pitching, rolling and yawing moments are obtained in the wind-axis frame through the use of a transformation matrix.

$$\begin{bmatrix} C_L \\ C_D \\ C_Y \end{bmatrix} = \begin{bmatrix} -SIN\alpha & 0 & COS\alpha \\ COS\beta COS\alpha & SIN\beta & COS\beta SIN\alpha \\ -SIN\beta COS\alpha & COS\beta & -SIN\beta SIN\alpha \end{bmatrix} \begin{bmatrix} C_{FX} \\ C_{FY} \\ C_{FZ} \end{bmatrix}$$

$$\begin{bmatrix} C_M \\ C_R \\ C_N \end{bmatrix} = \begin{bmatrix} -\sin\beta\cos\alpha & \cos\beta & -\sin\beta\sin\alpha \\ \cos\beta\cos\alpha & \sin\beta & \cos\beta\sin\alpha \\ -\sin\alpha & 0 & \cos\alpha \end{bmatrix} \begin{bmatrix} C_{MX} \\ C_{MY} \\ C_{MZ} \end{bmatrix}$$

The expressions for aerodynamic parameters are for steady flow only.

REFERENCES

1. Young, A.D., Executive Summary, Aerodynamic Characteristics of Controls, AGARD CP-262, May 1979.

2. Burgess, M. A., Schreffler, E.S., Hill, J. C., Osterbeck, P. G., Woodhead, G. E., "HAV-SPRINT: A Conceptual Design Computer Code for Hypersonic Vehicle Synthesis and Optimization," AIAA 87-2956, AIAA/AHS/ASEE Aircraft Design, Systems and Operations Meeting, Sept. 1987.

3. Hunt, J. L., "Hypersonic Airbreathing Vehicle Design (Focus on Aero-Space Plane) Hypersonics," Volume 1: Defining the Hypersonic Environment, Progress in Scientific Computing, Volume 8, Birkhauser, Boston, 1989.

4. Rao, D. M.; "Hypersonic Control Effectiveness Studies on Delta Wings With Trailing Edge Flaps," Ph.D. Dissertation, Univ. of London, May, 1970.

5. Bertin, J. J., "General Characterization of Hypersonic Flows," Hypersonics, Volume 1: Defining the Hypersonic Environment, Progress in Scientific Computing, Volume 8, Birkhauser, Boston, 1989.

6. Woods, W. C., Arrington, J. P., and Hamilton, H. H. II, "A Review of Preflight Estimates of Real-Gas Effects on Space Shuttle Aerodynamic Characteristics," Shuttle Performance: Lessons Learned, NASA Conference Publication 2283, Part I, March 1983.

7. Griffith, B. J., Maus, J. R., and Best, J. T., "Explanation of the Hypersonic Longitudinal Stability Problem - Lessons Learned," Shuttle Performance: Lessons Learned, NASA Conference Publication 2283, Part I, March 1983.

8. Kirsten, P. W., Richardson, D. F., and Wilson, C. M., "Predicted and Flight Test Results of Performance, Stability and Control of the Space Shuttle From Reentry to Landing," Shuttle Performance: Lessons Learned, NASA Conference Publication 2283, Part I, March 1983.

9. Findlay, J. T., Kelly, G. M., McConnell, J. G., "Shuttle 'Challenger' Aerodynamic Performance From Flight Data-Comparisons with Predicted Values and 'Columbia' Experience," AIAA 84-0485, 22nd Aerospace Sciences Meeting, January 1984.

10. Romere, P. O., and Young, J. C., "Space Shuttle Entry Longitudinal Aerodynamic Comparisons of Flight 2 with Preflight Predictions," Journal of Spacecraft and Rockets, Vol. 20, No. 6, November-December 1983, pp. 518-523.

11. Maus, J. R., Griffith, B. J., and Szema, K. Y., "Hypersonic Mach Number and Real Gas

Effects on Space Shuttle Orbiter Aerodynamics," Journal of Spacecraft and Rockets," Vol 21, No. 2, March-April 1984, pp. 136-141.

12. Bruno, C., "Real Gas Effects," Hypersonics, Volume 1, Defining the Hypersonic Environment, Progress in Scientific Computing, Volume 8, Birkhauser, Boston 1989.

13. Koppenwallner, G., "Low Reynolds Number Influence on Aerodynamic Performance of Hypersonic Lifting Vehicles," AGARD CP-428, April, 1987.

14. Neumann, R. D., "Defining the Aerothermodynamic Methodology," Hypersonics, Volume 1: Defining the Hypersonic Environment, Progress in Scientific Computing, Volume 8, Birkhauser, Boston 1989.

15. Ozoroski, L. P., "Evaluation of Methods for Predicting the Forces and Moments Generated by Control Surface Deflections on Hypersonic Vehicles," Master's Thesis, Department of Aerospace Engineering, The Pennsylvania State University, May 1990.

16. Trella, M., "Introduction to the Hypersonic Phenomena of Hemes," Hypersonics, Volume 1: Defining the Hypersonic Environment, Progress in Scientific Computing, Volume 8, Birkhauser, Boston 1989.

17. Anderson, J. D. Jr., "Hypersonic and High Temperature Gas Dynamics," McGraw-Hill Book Company, New York, 1989.

18. Morkovin, M. V., "Instability, Transition to Turbulence and Predictability," AGARD-AG-236, Fluid Dynamics 2-4, Panel Symposium on "Laminar-Turbulent Transition," May 2-4, 1977.

19. Morkovin, M. V., "Critical Evaluation of Transition From Laminar to Turbulent Shear Layers with Emphasis on Hypersonic Traveling Bodies," AFFDL-TR-68-149, March 1969.

20. Kendall, J. M., "Wind Tunnel Experiments Relating to Supersonic and Hypersonic Boundary-Layer Transition," AIAA Journal, Vol. 13, NO. 3, March 1975, pp. 290-299.

21. Beckwith, I. E., "Development of a High Reynolds Number Quiet Tunnel for Transition Research," AIAA Journal, Vol. 13, No. 3, March 1975, pp. 300-314.

22. Howe, J. T., "Some Fluid Mechanical Problems Related to Subsonic and Supersonic Aircraft," NASA SP-183, 1968.

23. Jones, J. L., "The Transonic Reynolds Number Problem," NASA CP-2009, Workshop on High Reynolds Number Research, October 27-28, 1976, pp. 1-18.

24. Raj, P., Brennen, J.E., Keen, J.M., Long, L.N., Sikora, J.S., and Singer, S.W., "Three-Dimensional Euler Aerodynamic Method (TEAM)," Vol. 1, 2, and 3, AFWAL-TR-87-3074, WPAFB, Ohio, October 1987.

25. Newton, Sir I.; Principia, Univ. of Calif. Press, 1687.

26. Lees, L., "Hypersonic Flow," Fifth International Aeronautical Conference, Los Angeles, 1955, pp. 241-276. Published by The Institute of Aeronautical Sciences, Through the Sherman M. Fairchild Fund.

27. Anderson, J. D., Fundamentals of Aerodynamics, McGraw-Hill Book Co., New York, 1984.

28. Landrum, E. J., "Wind-Tunnel Pressure Data at Mach Numbers from 1.6 to 4.63 for a Series of Bodies of Revolution at Angles of Attack from -4° to 60°," NASA TM X-3558, October 1977.

29. Schindel, L. H., "Design of High Performance Hypersonic Missiles," AIAA Paper 82-0391, 20th Aerospace Sciences Meeting, Orlando, Florida, January 11-14, 1982.

30. L.N. Long; "The Off-Design Performance of Hypersonic Waveriders," Journal of Aircraft, Vol. 27, No. 7, July, 1990.

31. Rasmussen, M. L., Jischke, M. C., and Daniel, D. C., "Experimental Forces and Moments on Core-Derived Waveriders for M_∞ = 3 to 5," Journal of Spacecraft and Rockets, Volume 19, No. 6, December, 1982, pp. 592-598.

32. Keener, E. R., "Pressure-Distribution Measurements on a Transonic Low-Aspect Ratio Wing," NASA TM 86683, September 1985.

33. L.N. Long, "Navier-Stokes and Monte Carlo Results for Hypersonic Flows," AIAA Journal, Vol. 29, No. 2, Feb., 1991.

34. Bird, G. A., Molecular Gas Dynamics, Clarendon Press, 1976.

35. Holden, M. S., "Studies of the Heat Transfer and Flow Characteristics of Rough and Smooth Indented Noseshapes - Part I, Steady Flows," AIAA Paper No. 86-0384, 1986.

36. Bonner, E., Clever, W., and Dunn, K., "Aerodynamic Preliminary Analysis System II - Part I, Theory," NASA CR-165627, 1981.

37. Gentry, A.E., "Hypersonic Arbitrary-Body Aerodynamic Computer Program (Mark III Version), Vol. 1 - User's Manual," Report DAC 61552, McDonnell-Douglas Corporation, April 1968.

38. Maughmer, M., Ozoroski, L., and Straussfogel, D., "Validation of Methods for Predicting Hypersonic Vehicle Control Effectors," NASP CR-1104, July, 1990. (see also: Progress Report-- Part I, NASA Grant NAG 1-849, April 1990.)

39. Maughmer, M.D., Ozoroski, L., Straussfogel, D., and Long, L.; "Validation of Engineering Methods for Predicting Hypersonic Vehicle Control Forces and Moments," AIAA Paper No. 91-2845, Presented at the AIAA Atmospheric Flight Mechanics Conference, New Orleans, Aug, 1991.

40. Maughmer, M.D., Ozoroski, L., Straussfogel, D., and Long, L.; "Validation of Engineering Methods for Predicting Hypersonic Vehicle Control Forces and Moments," to appear in Journal of Guidance, Control, and Dynamics, 1993.

41. Hankey, W.; Re-Entry Aerodynamics, AIAA Education Series, Wash., D.C., 1988.

42. Pagano, P., "Evaluation of Simple Hypersonic Methods for Predicting Aerodynamic Coefficients and Control Surface Effectiveness," M.S. Thesis, Department of Aerospace Engineering, Penn State University, May 1993.

43. Guilmette, N.H., "Improvements to Impact Methods for Hypersonic Control Deflections," M.S. Thesis, to be presented to the Department of Aerospace Engineering, Penn State University, May, 1993.

44. Vincenti, W. G., and Kruger, C. H., Jr., Introduction to Physical Gas Dynamics, Krieger Press, 1986.

45. Srinivasan, S., Tannehill, J. C., and Weilmuenster, K. J., "Simplified Curve Fits for the Thermodynamic Properties of Equilibrium Air," NASA Reference Publication 1181, August 1987.

46. Srihivasan, S. and Tannehill, J. C., "Simplified Curve Fits for the Transport Properties of Equilibrium Air," NASA Contractor Report 178411, December 1987.

47. Baldwin, B. S. and Lomax, H., "Thin Layer Approximation and Algebraic Model for Separated Turbulent Flows," AIAA Paper 78-275, January 1978.

48. Gnoffo, P. A., McCandless, R. S. and Yec, H. C., "Enhancements to Program LAURA for Computation of Three-Dimensional Hypersonic Flow," AIAA Paper 87-0280, 25th Aerospace Sciences Meeting, Reno, Nevada, January 12-15, 1987.

49. Gnoffo, P. A., "Application of Program LAURA to Three-Dimensional AOTV Flow Fields," AIAA Paper 86-0565, 24th Aerospace Sciences Meeting, Reno, Nevada, January 9-12, 1984.

50. Tannehill, J. C., Holst, T. L., and Rakish, J. V., "Numerical Computation of Two-Dimensional Viscous Blunt Body Flows with an Impinging Shock," AIAA Paper 75-154, Pasadena, California, 1975.

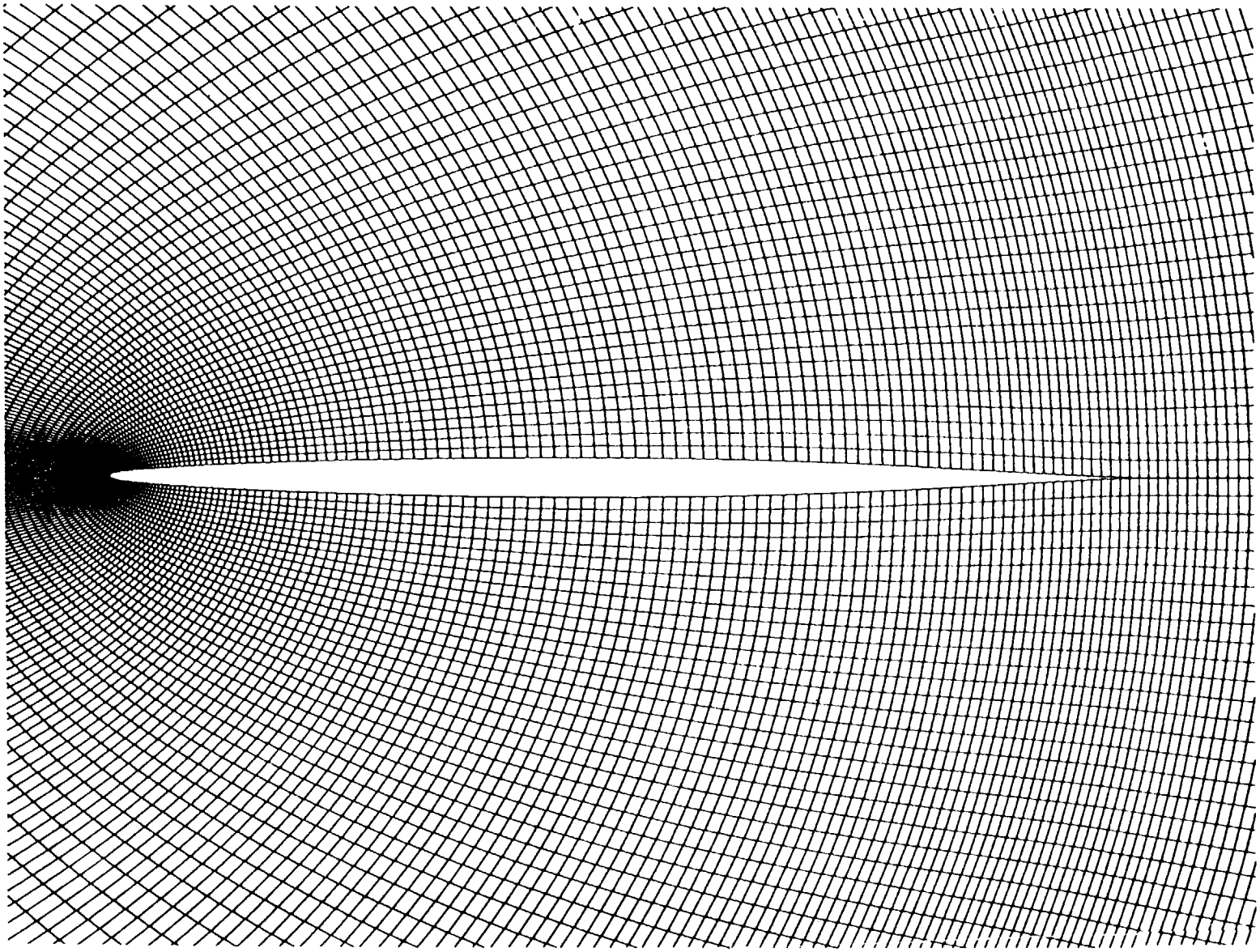

Figure 1: The TEAM Code Inviscid Grid

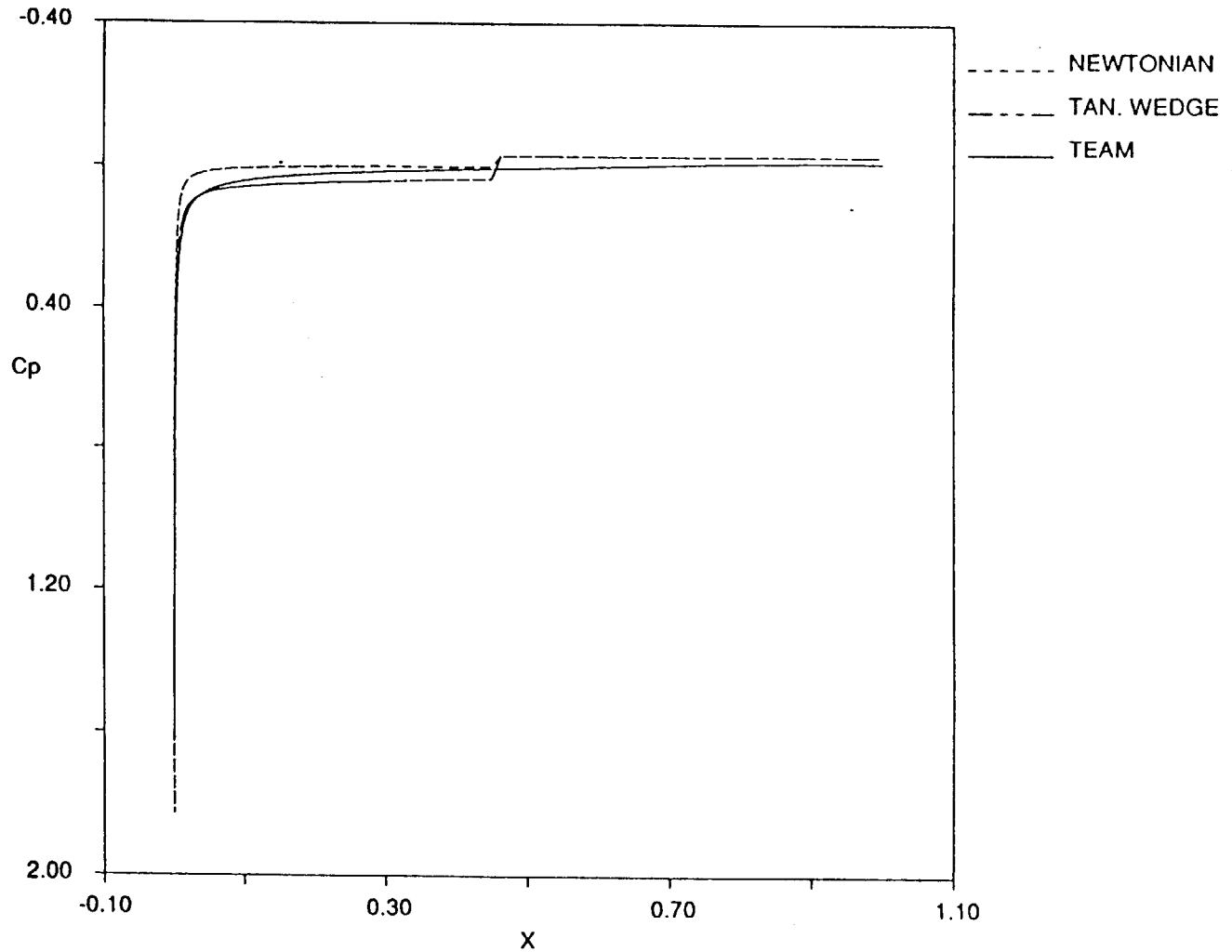

Figure 2a: Coefficient of Pressure on the Surface: M = 6.83, α = 0°, δ = 0°, Inviscid Perfect Gas

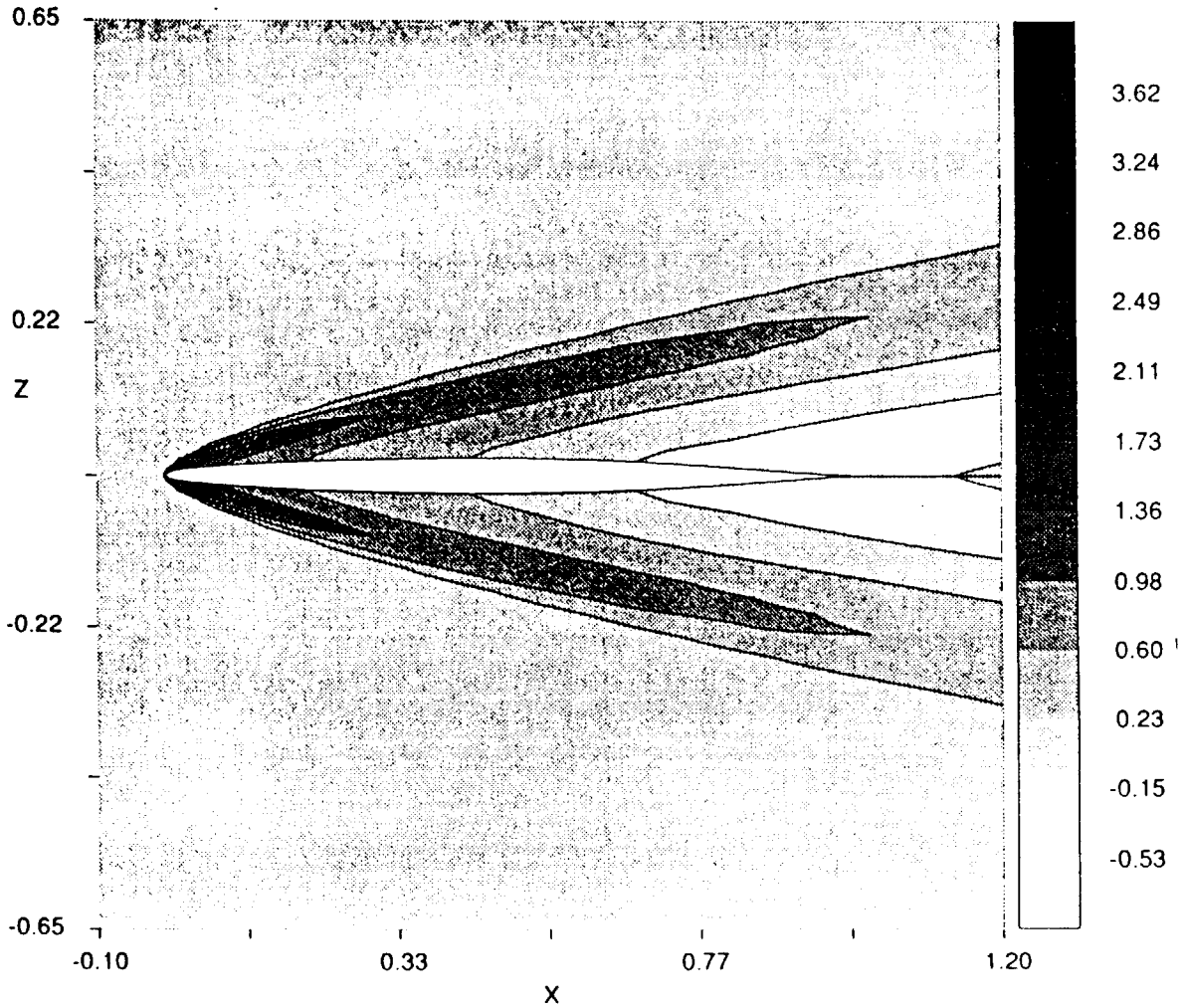

Figure 2b: TEAM Flowfield Results, Natural Log of Static Pressure Ratio: M = 6.83, α = 0°, δ = 0°, Inviscid Perfect Gas

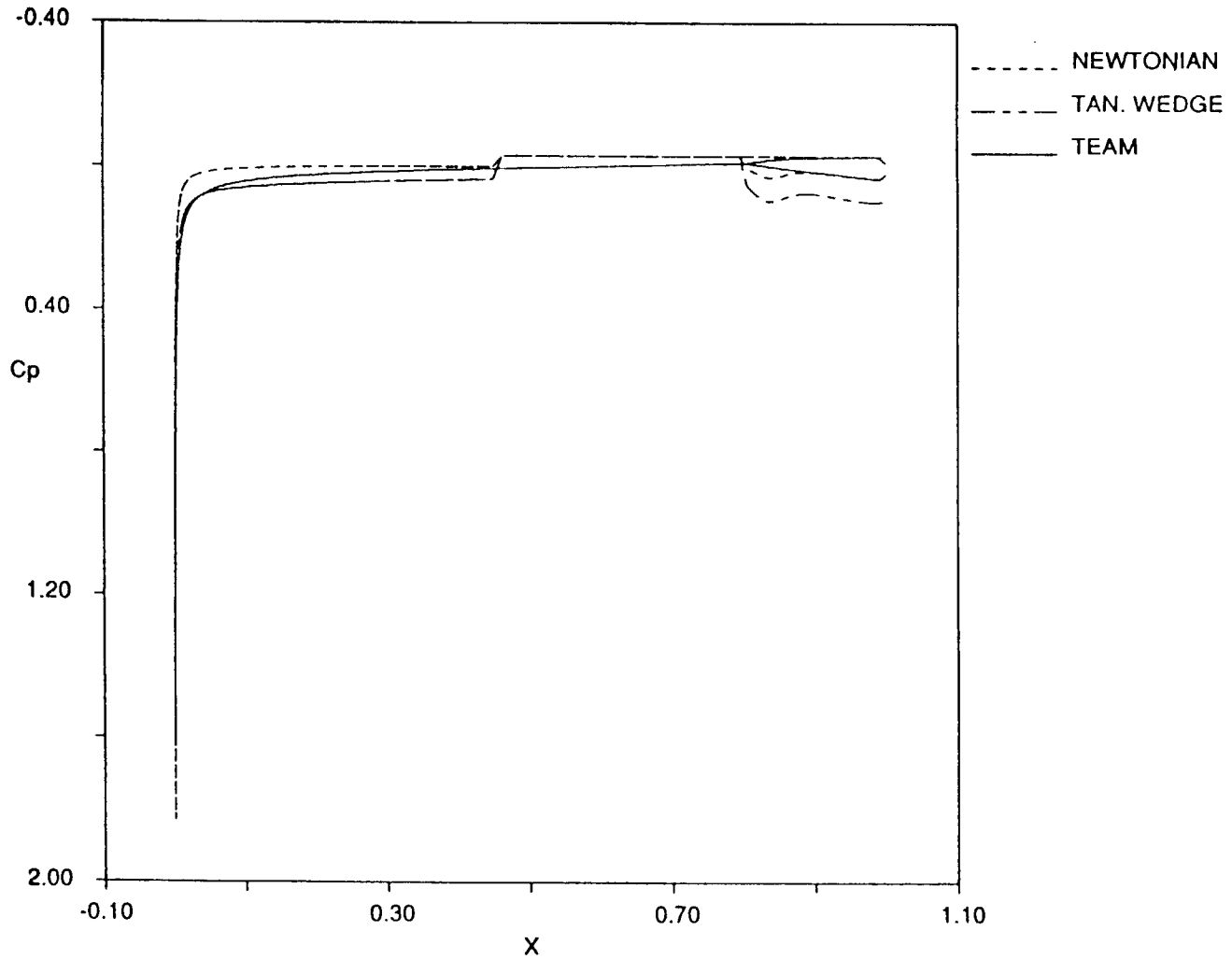

Figure 3a: Coefficient of Pressure on the Surface: M = 6.83, α = 0°, δ = 10°, Inviscid Perfect Gas

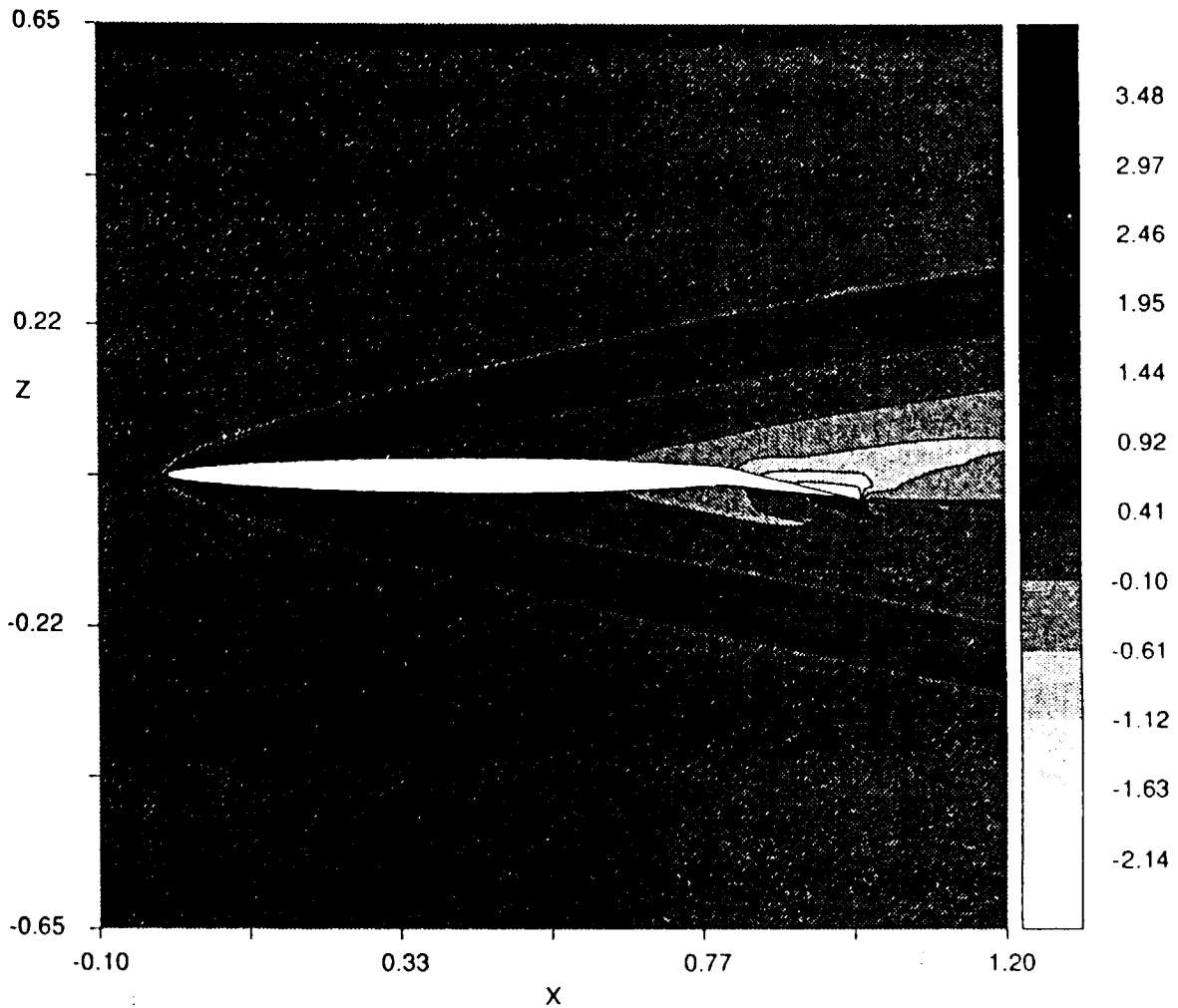

Figure 3b: TEAM Flowfield Results, Natural Log of Static Pressure Ratio: M = 6.83, α = 0°, δ = 10°, Inviscid Perfect Gas

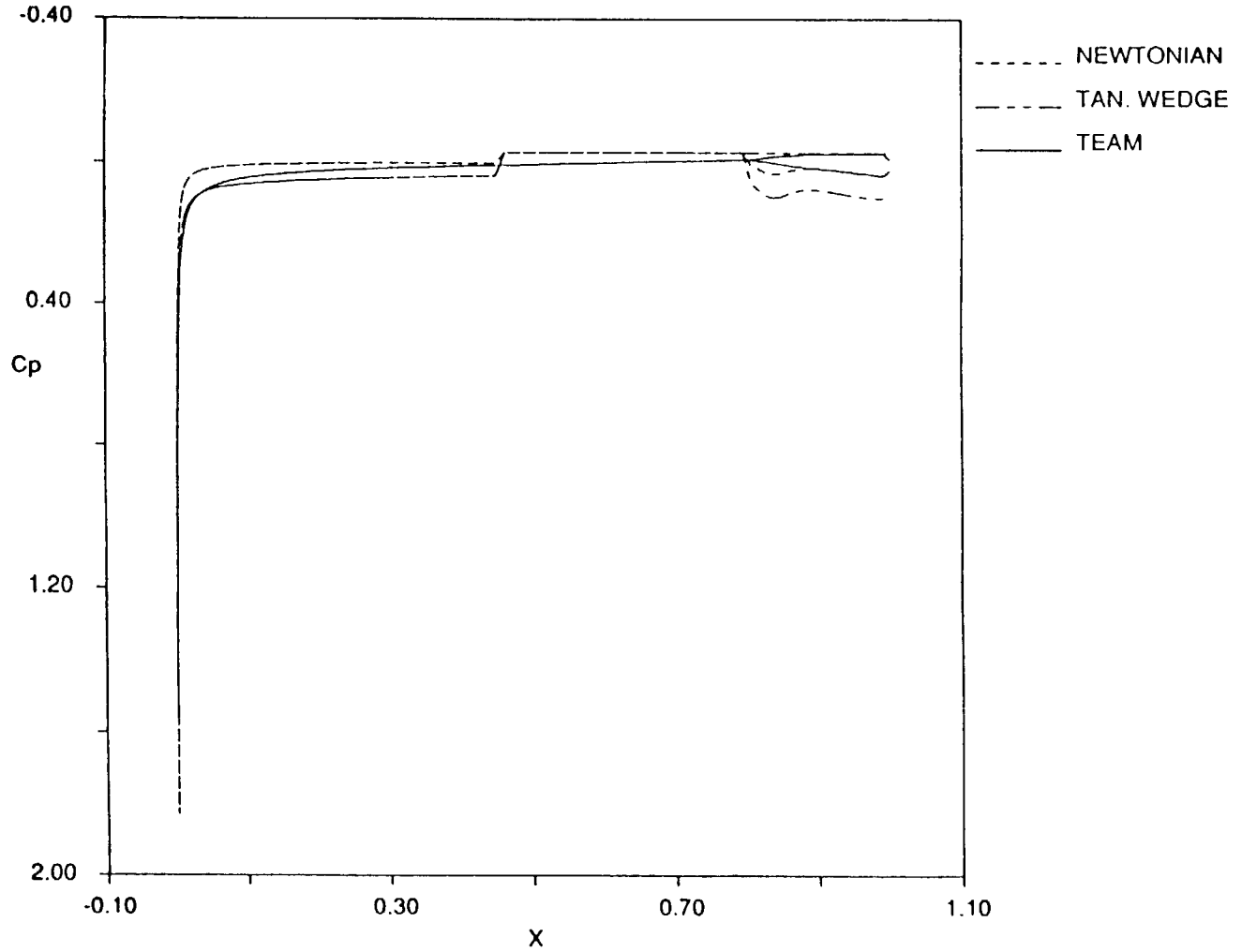

Figure 4a: Coefficient of Pressure on the Surface: M = 6.83, α = 0°, δ = -10°, Inviscid Perfect Gas

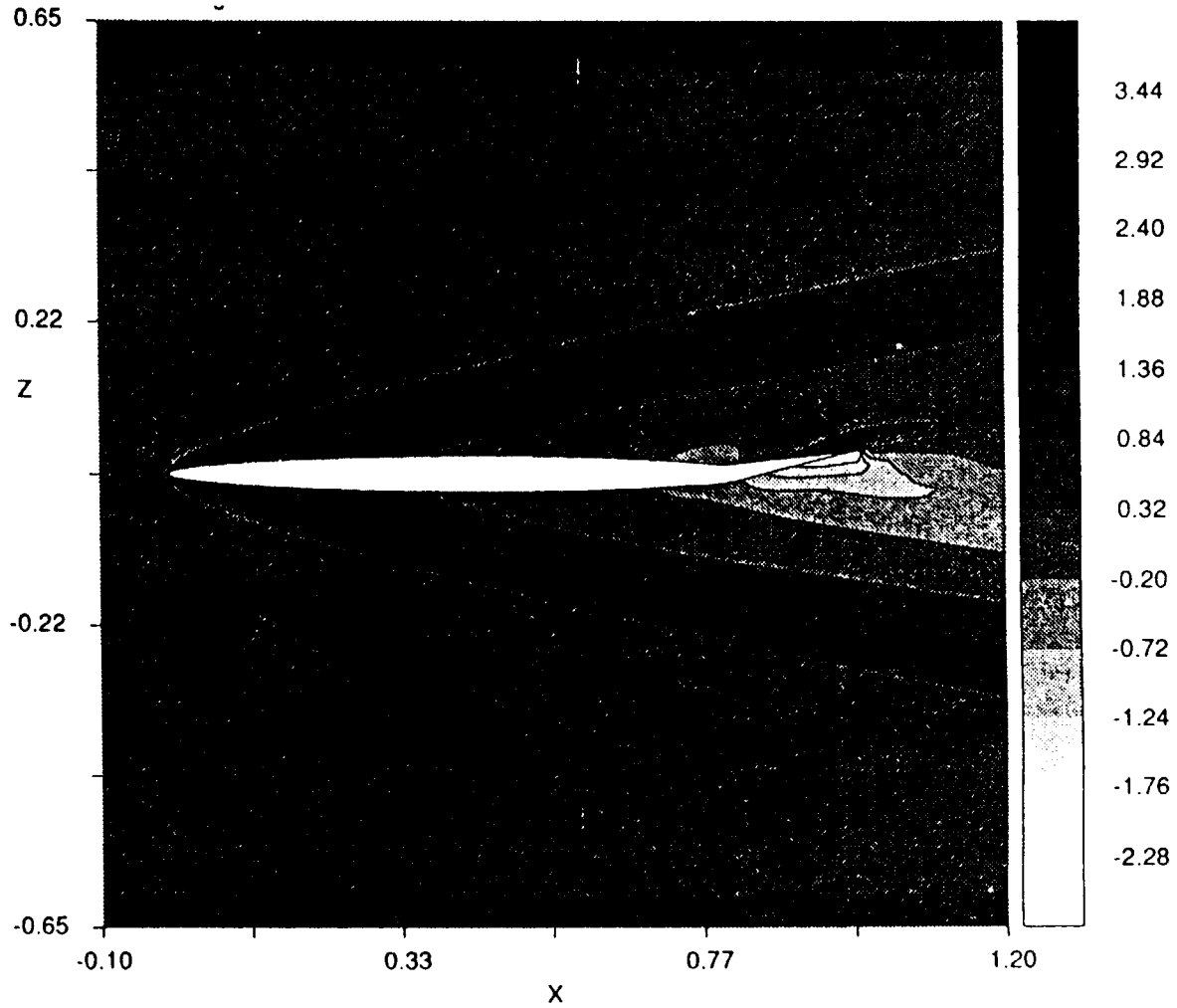

Figure 4b: TEAM Flowfield Results, Natural Log of Static Pressure Ratio: M = 6.83, α = 0°, δ = -10°, Inviscid Perfect Gas

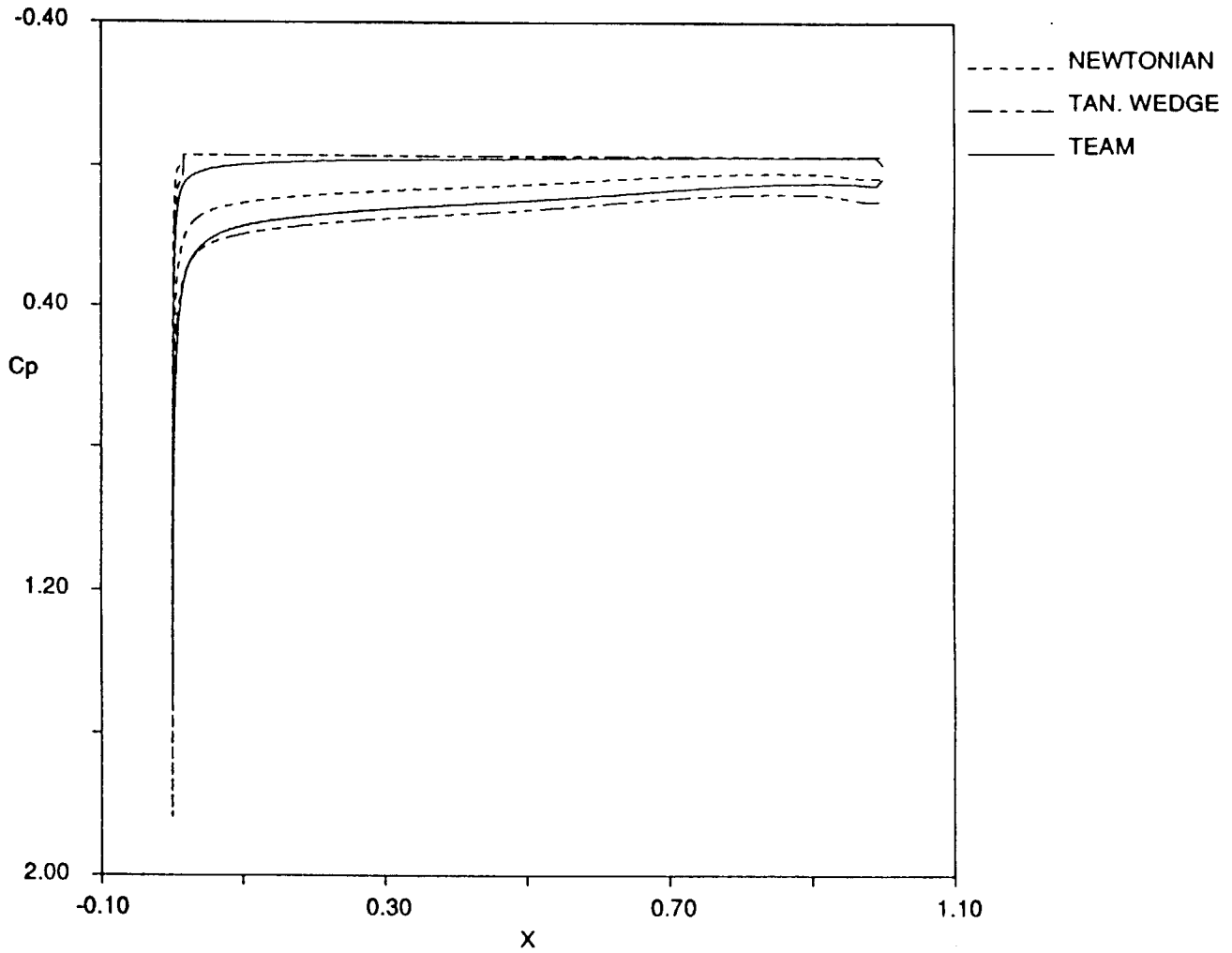

Figure 5a: Coefficient of Pressure on the Surface: M = 6.83, α = 10°, δ = 0°, Inviscid Perfect Gas

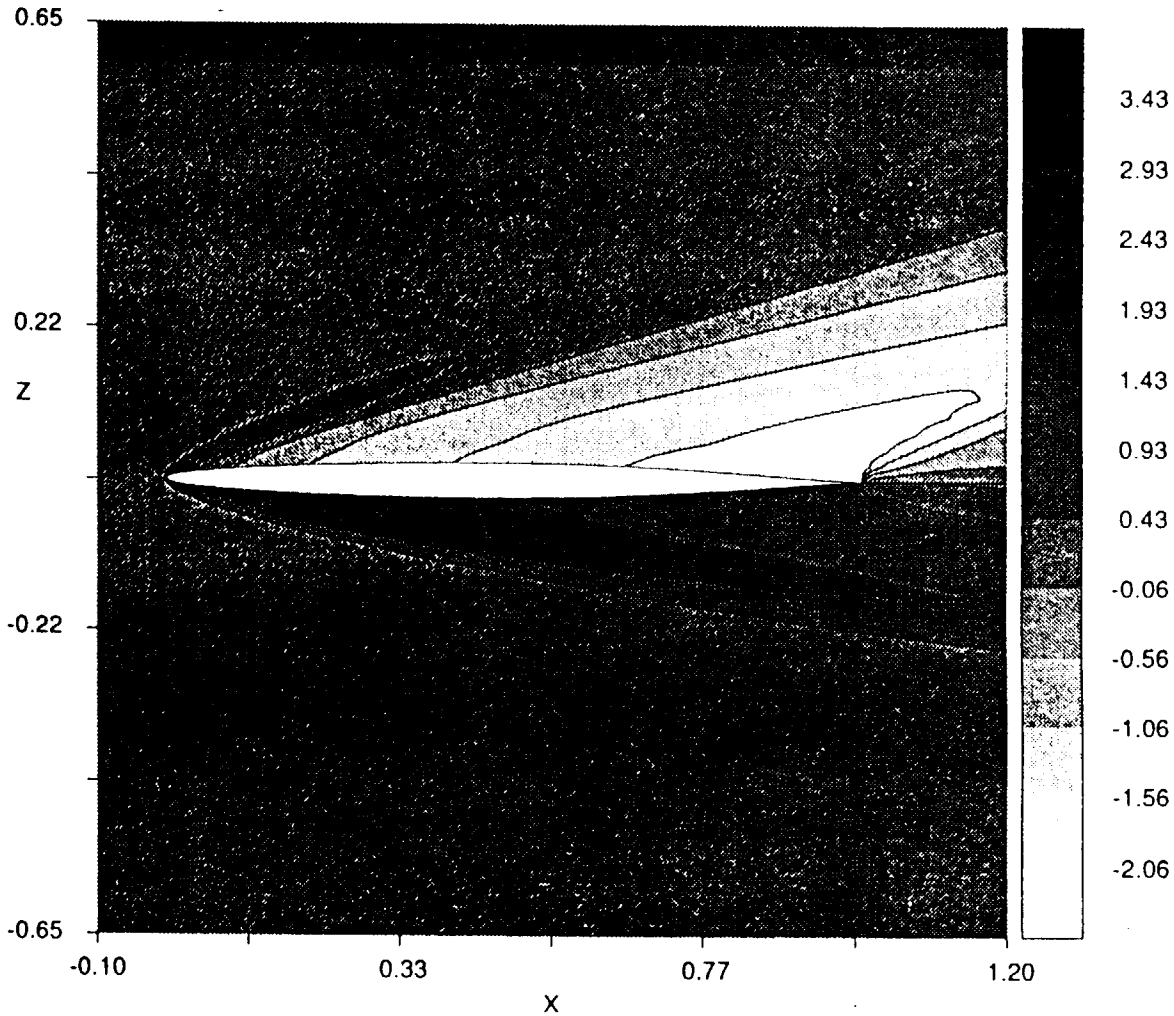

Figure 5b: TEAM Flowfield Results, Natural Log of Static Pressure Ratio: M = 6.83, α = 10°, δ = 0°, Inviscid Perfect Gas

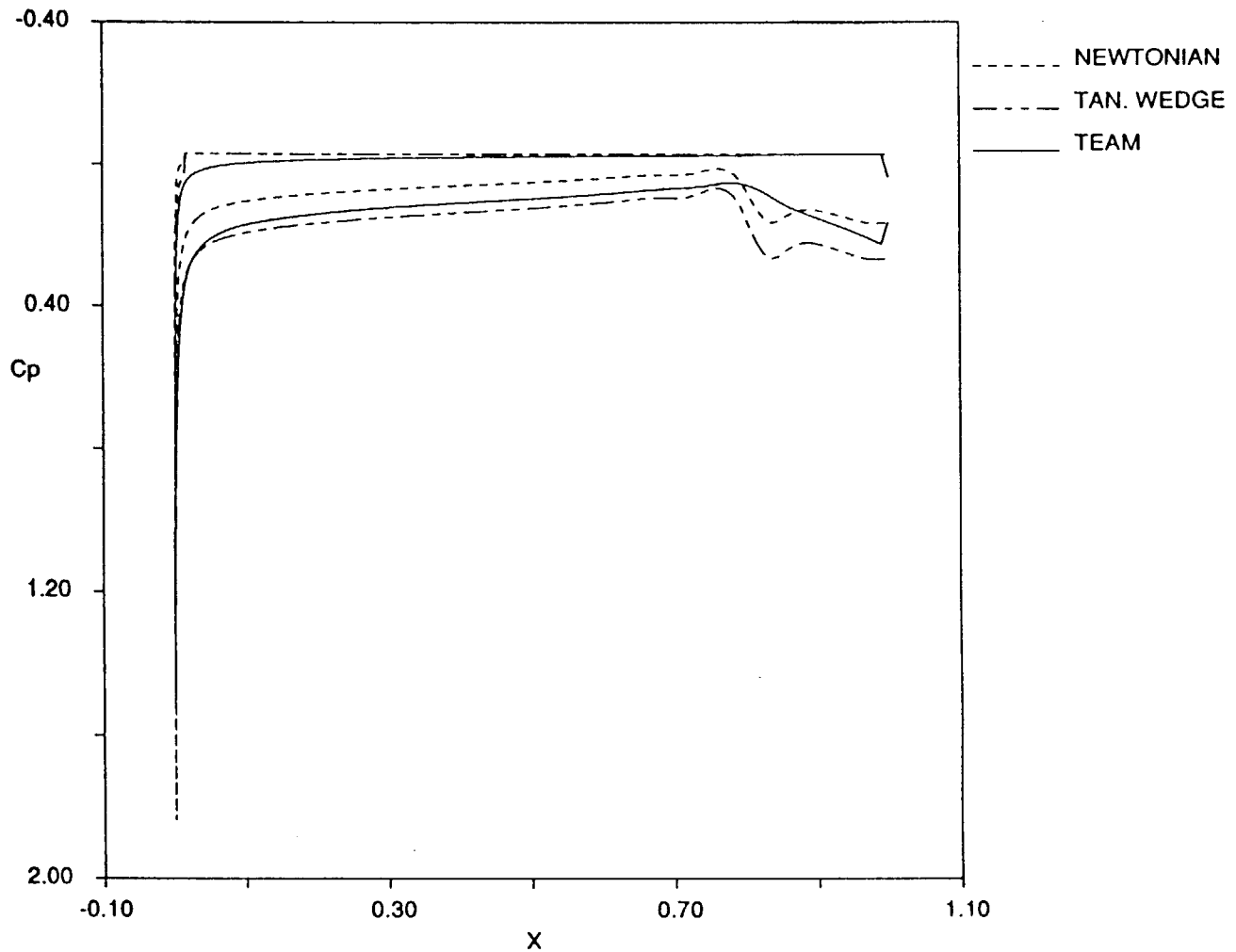

Figure 6a: Coefficient of Pressure on the Surface: M = 6.83, α = 10°, δ = 10°, Inviscid Perfect Gas

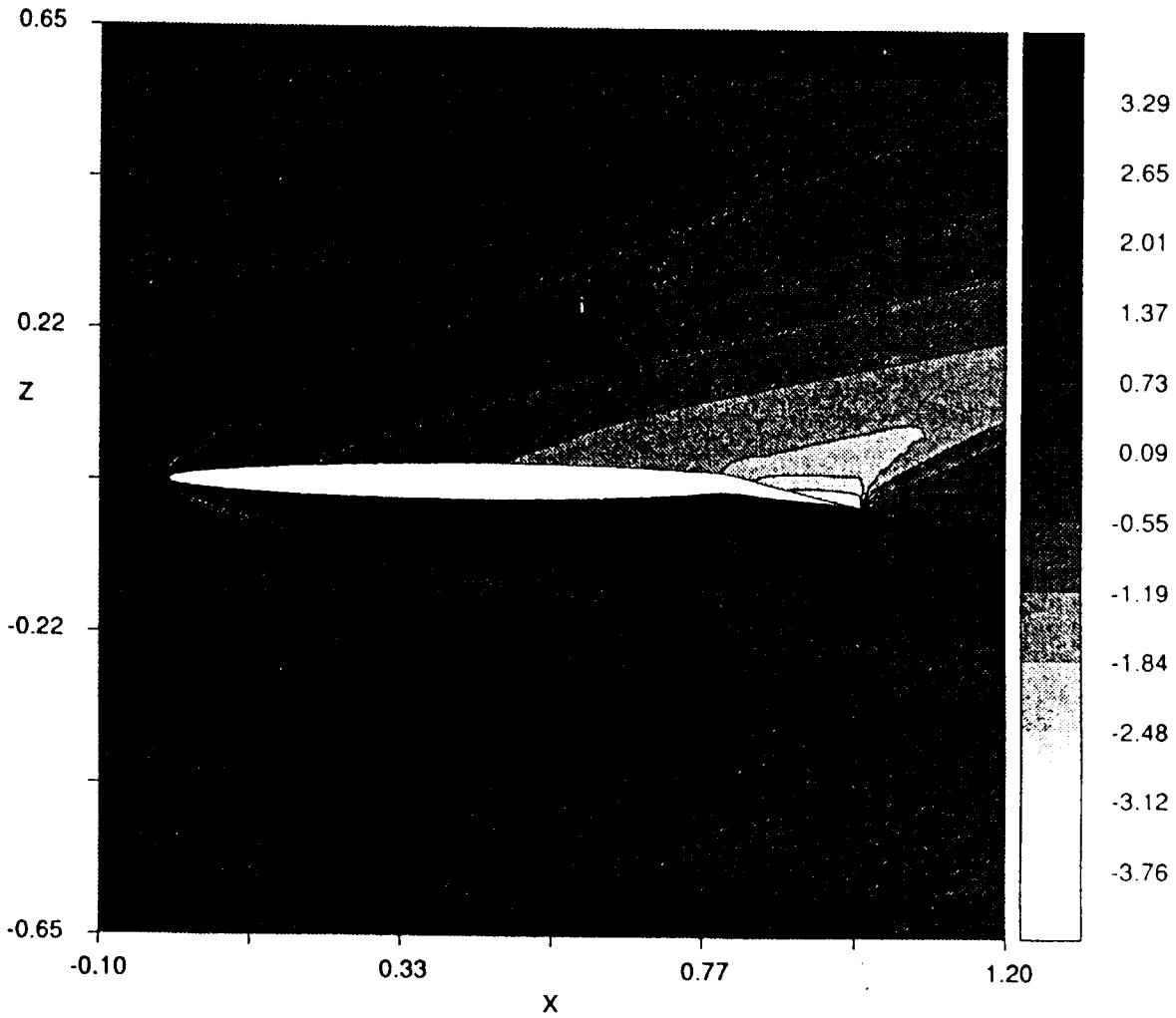

Figure 6b: TEAM Flowfield Results, Natural Log of Static Pressure Ratio: M = 6.83, α = 10°, δ = 10°, Inviscid Perfect Gas

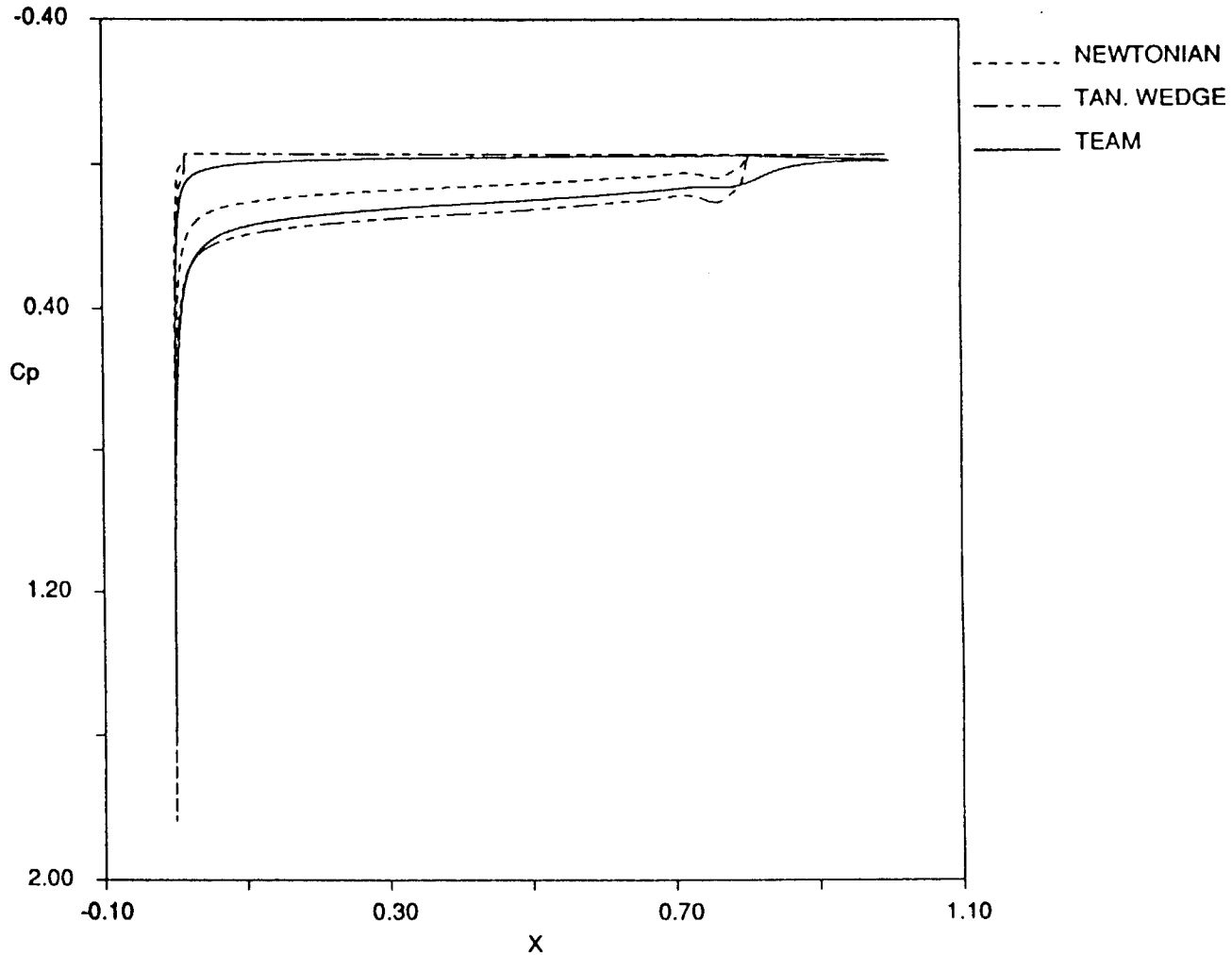

Figure 7a: Coefficient of Pressure on the Surface: M = 6.83, α = 10°, δ = -10°, Inviscid Perfect Gas

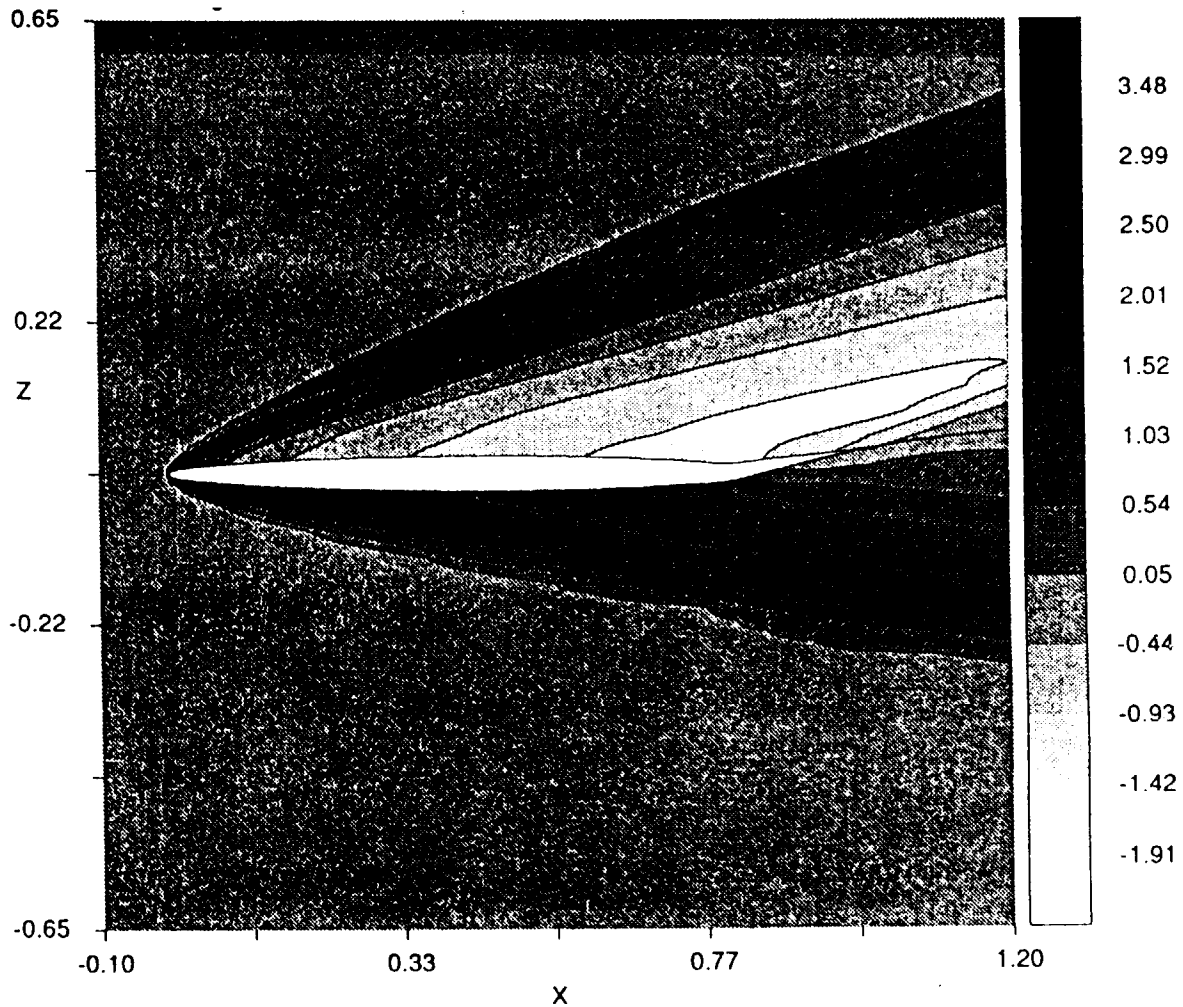

Figure 7b: TEAM Flowfield Results, Natural Log of Static Pressure Ratio: M = 6.83, α = 10°, δ = -10°, Inviscid Perfect Gas

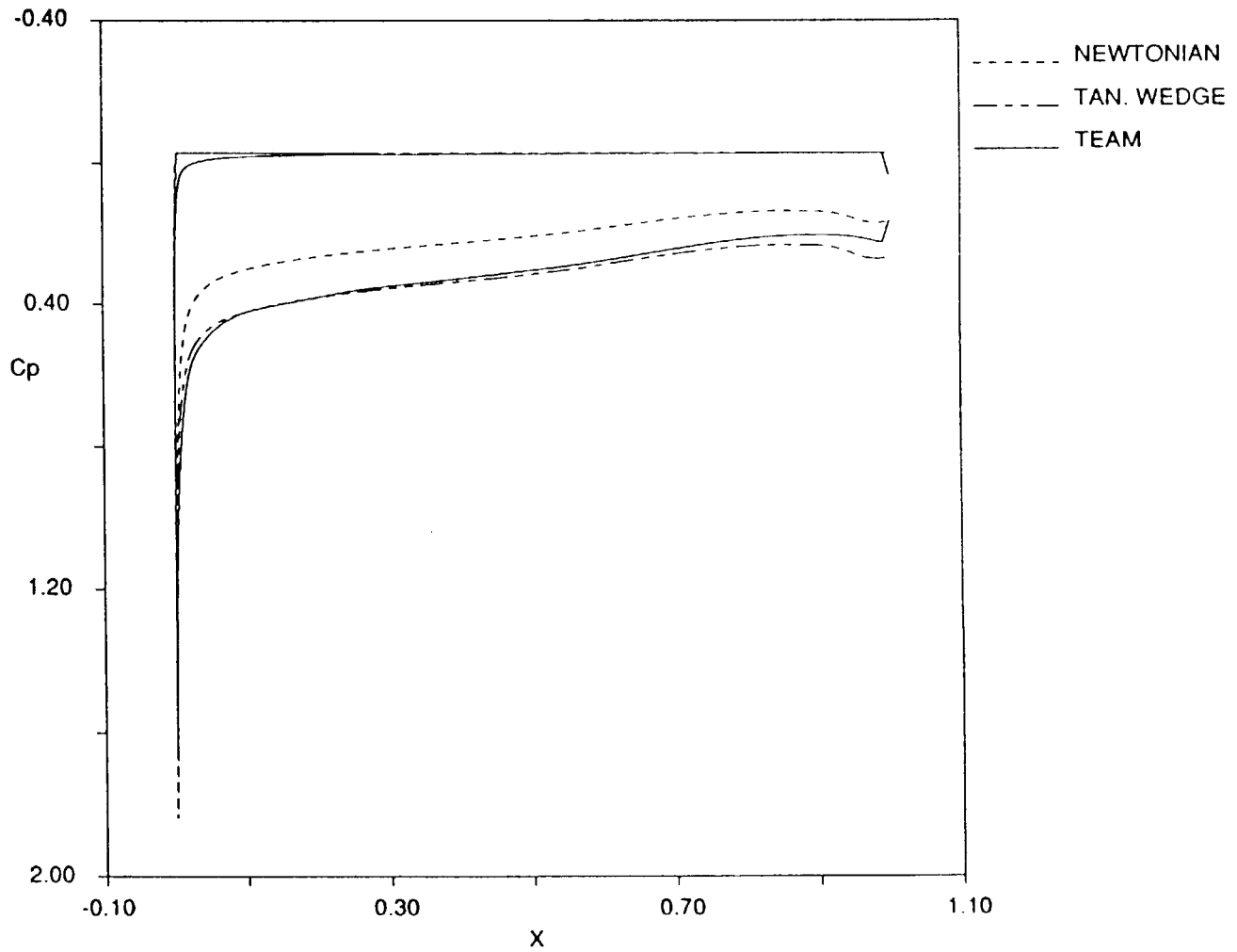

Figure 8a: Coefficient of Pressure on the Surface: M = 6.83, α = 20°, δ = 0°, Inviscid Perfect Gas

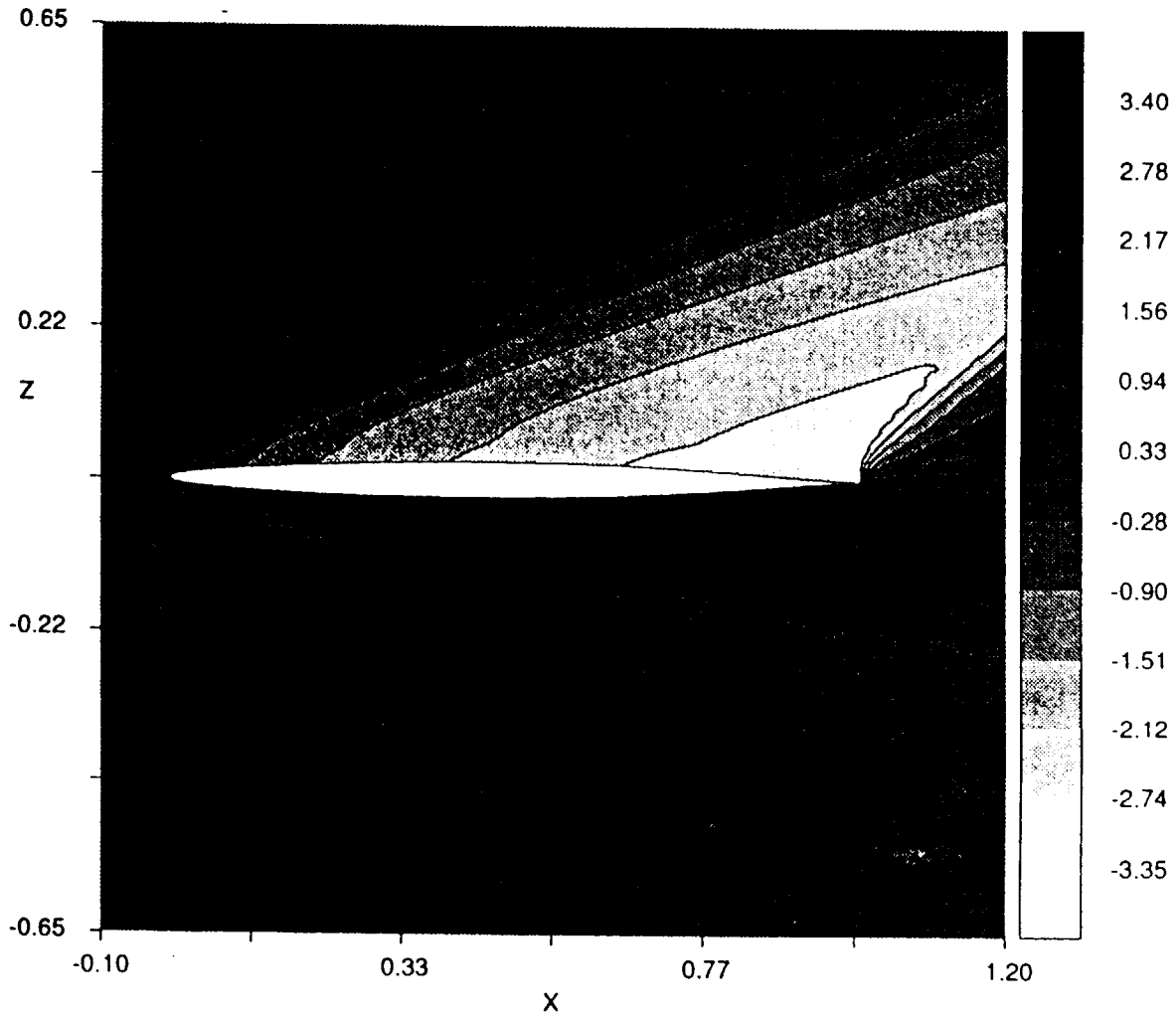

Figure 8b: TEAM Flowfield Results, Natural Log of Static Pressure Ratio: M = 6.83, α = 20°, δ = 0°, Inviscid Perfect Gas

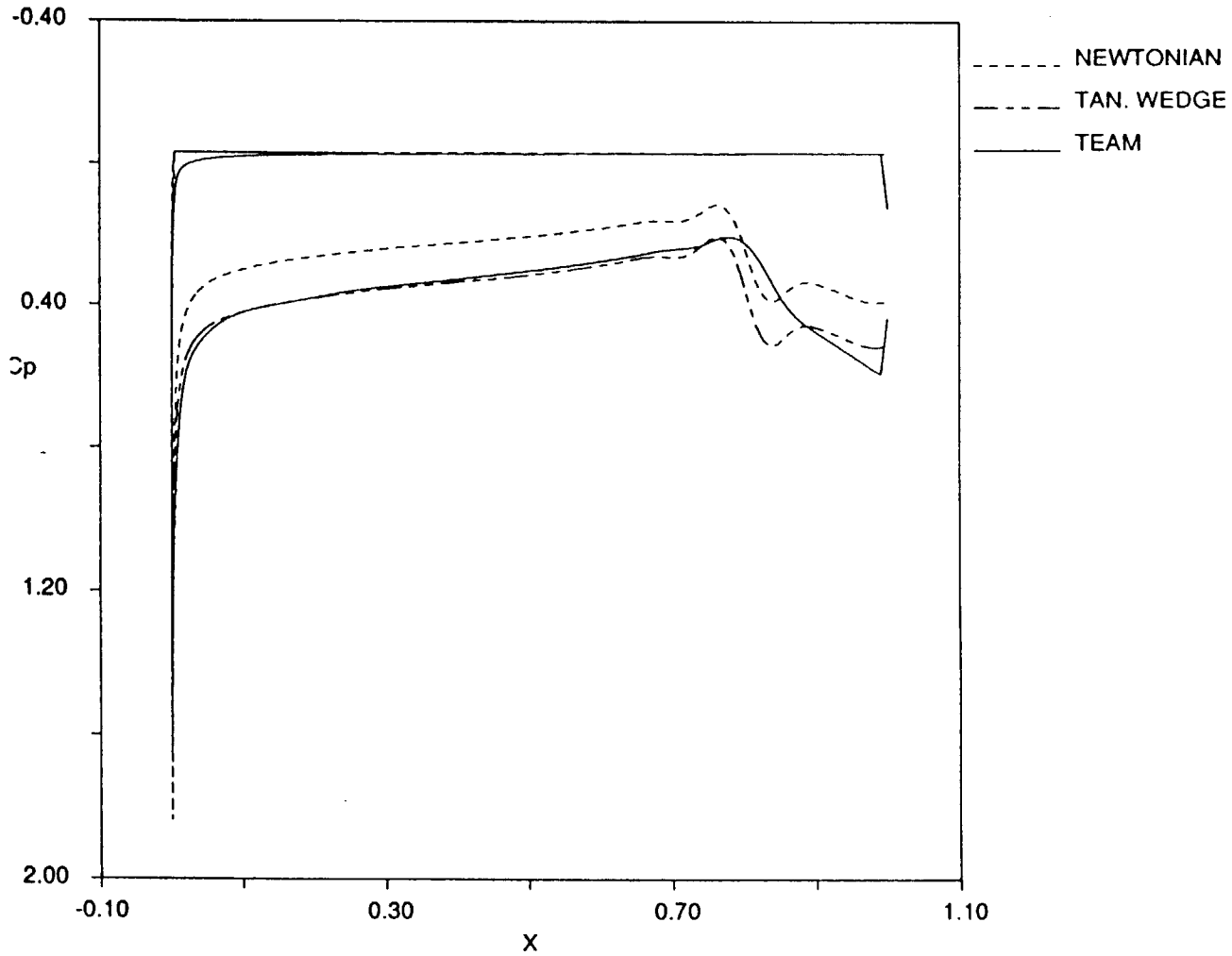

Figure 9a: Coefficient of Pressure on the Surface: M = 6.83, α = 20°, δ = 10°, Inviscid Perfect Gas

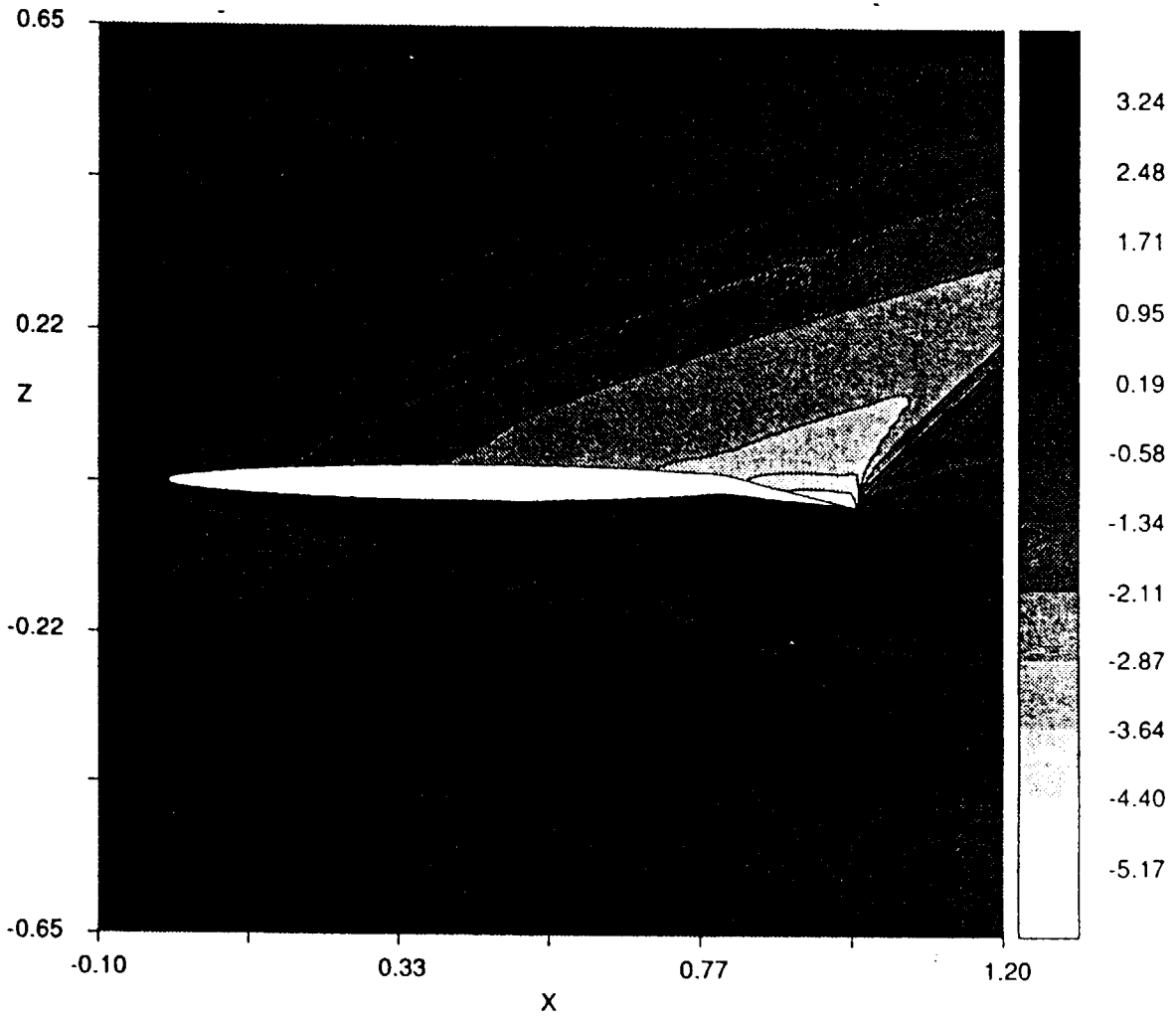

Figure 9b: TEAM Flowfield Results, Natural Log of Static Pressure Ratio: M = 6.83, α = 20°, δ = 10°, Inviscid Perfect Gas

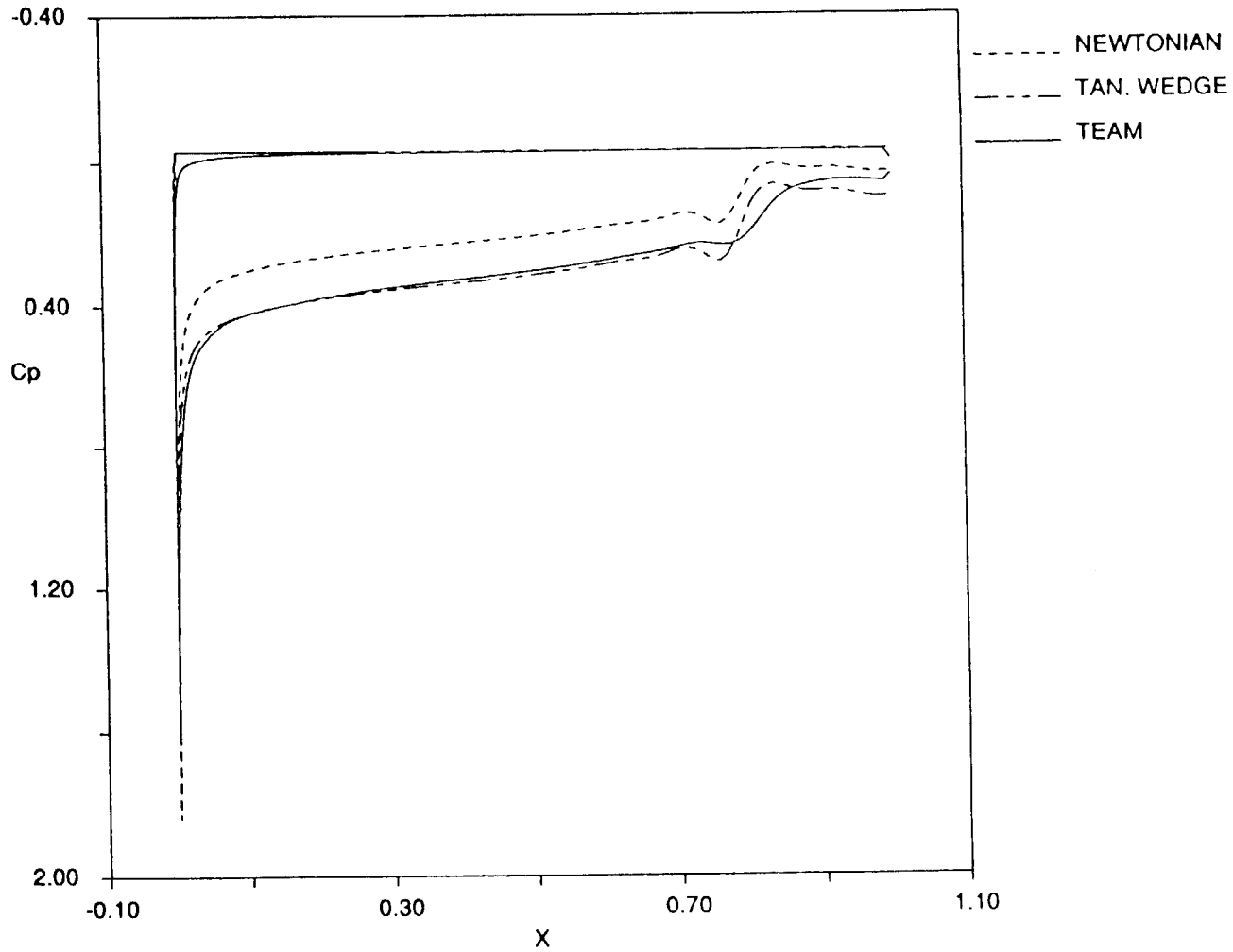

Figure 10a: Coefficient of Pressure on the Surface: M = 6.83, α = 20°, δ = -10°, Inviscid Perfect Gas

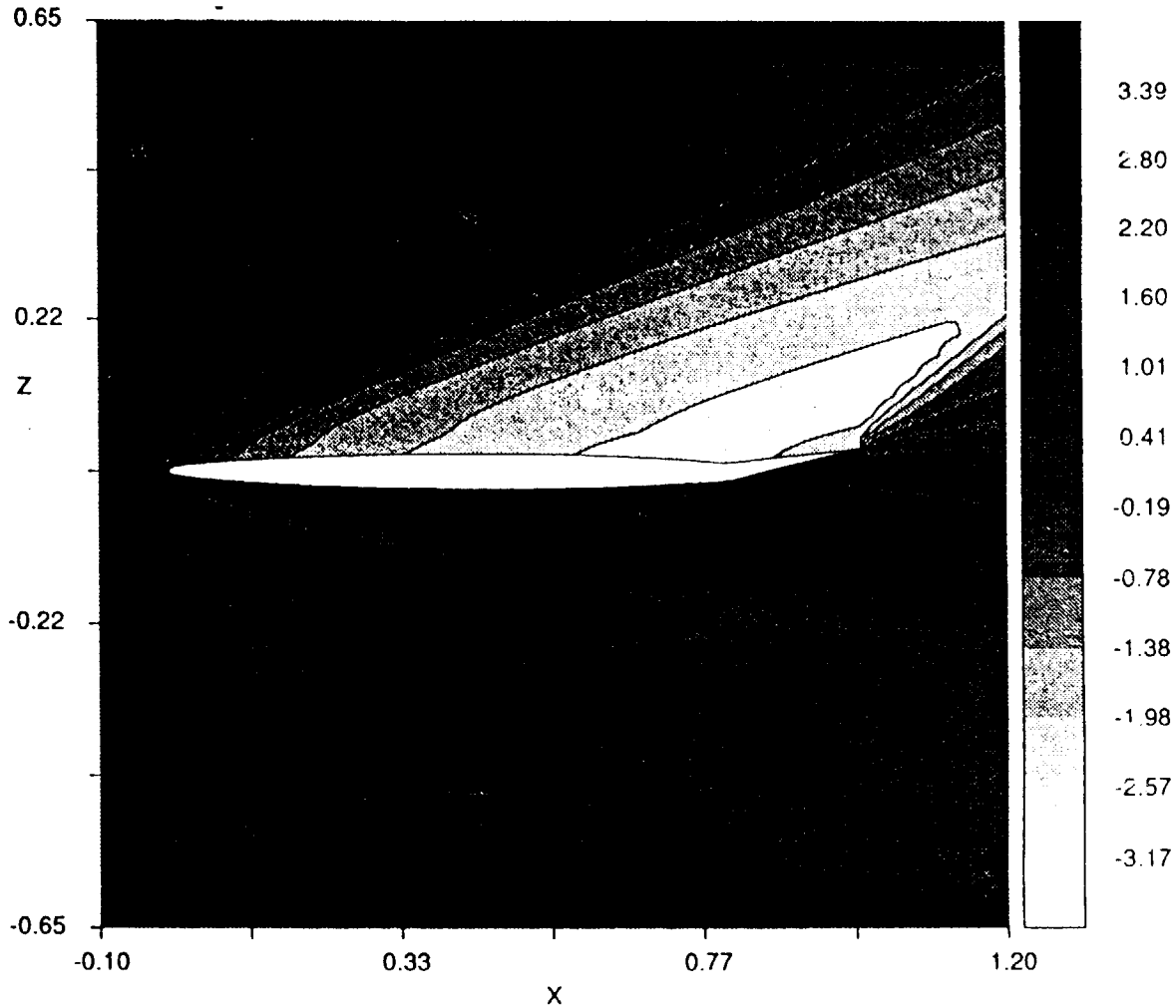

Figure 10b: TEAM Flowfield Results, Natural Log of Static Pressure Ratio: M = 6.83, α = 20°, δ = -10°, Inviscid Perfect Gas

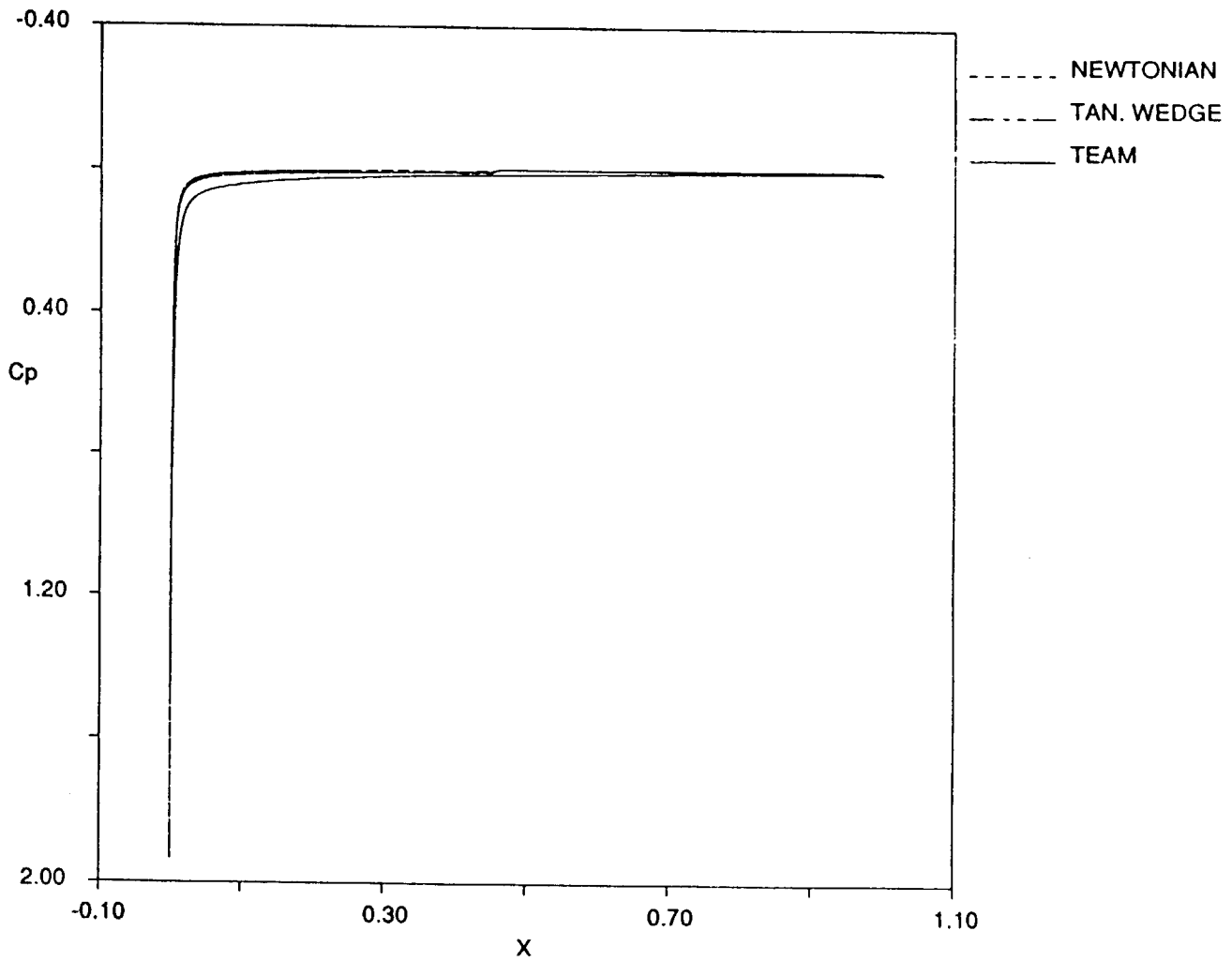

Figure 11a: Coefficient of Pressure on the Surface: M = 23.0, α = 0°, δ = 0°, Inviscid Perfect Gas

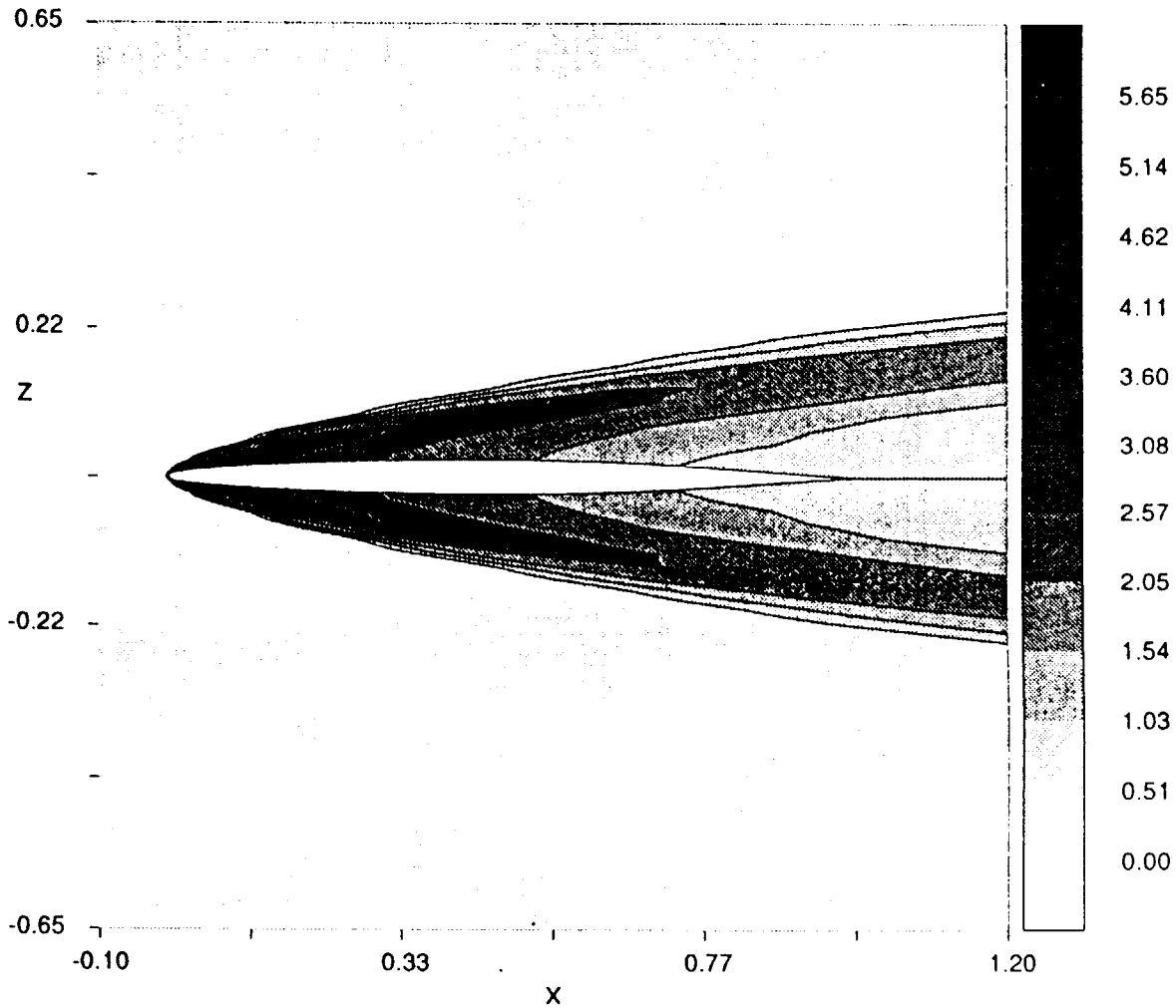

Figure 11b: TEAM Flowfield Results, Natural Log of Static Pressure Ratio: M = 23.0, α = 0°, δ = 0°, Inviscid Perfect Gas

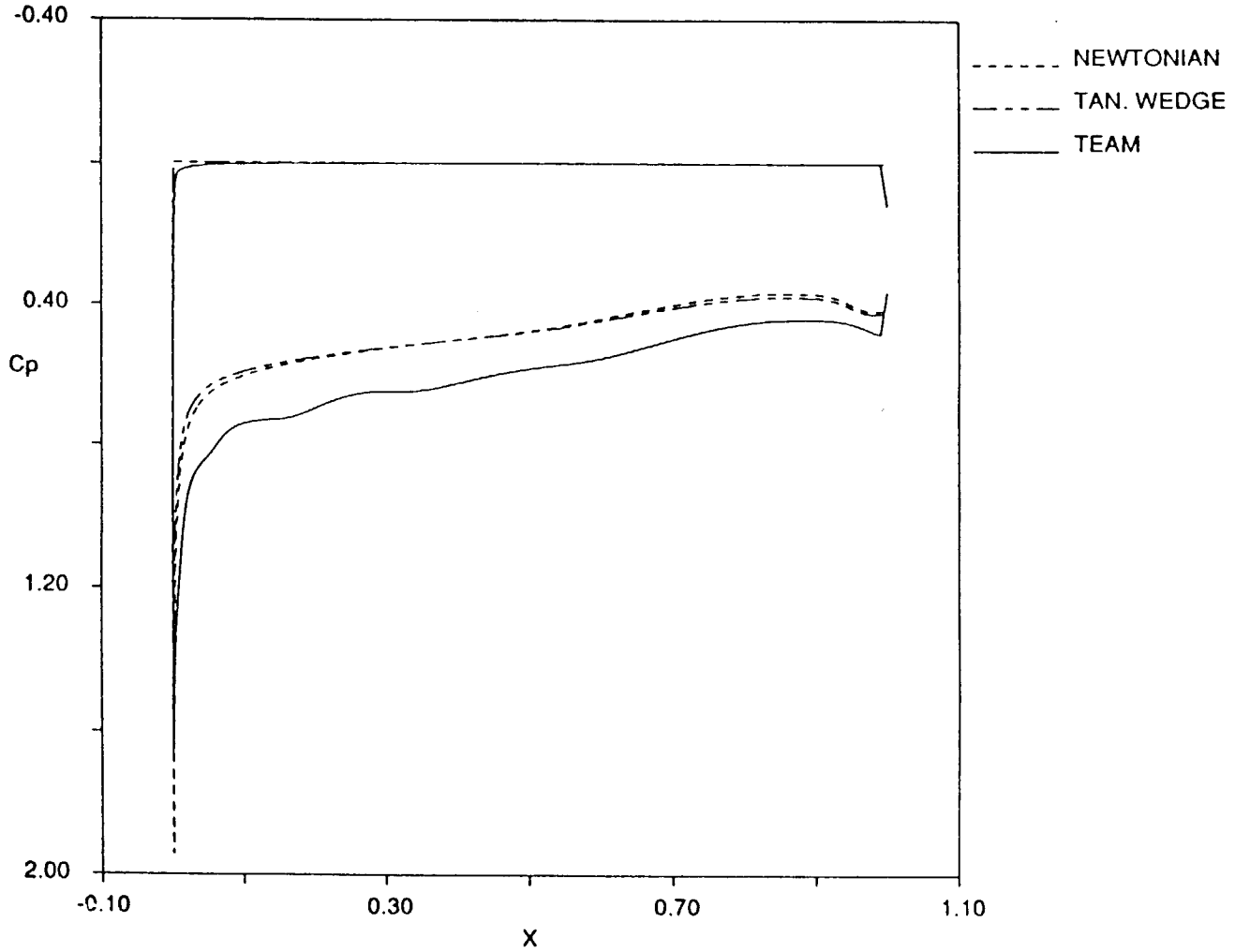

Figure 12a: Coefficient of Pressure on the Surface: M = 23.0, α = 30°, δ = 0°, Inviscid Perfect Gas

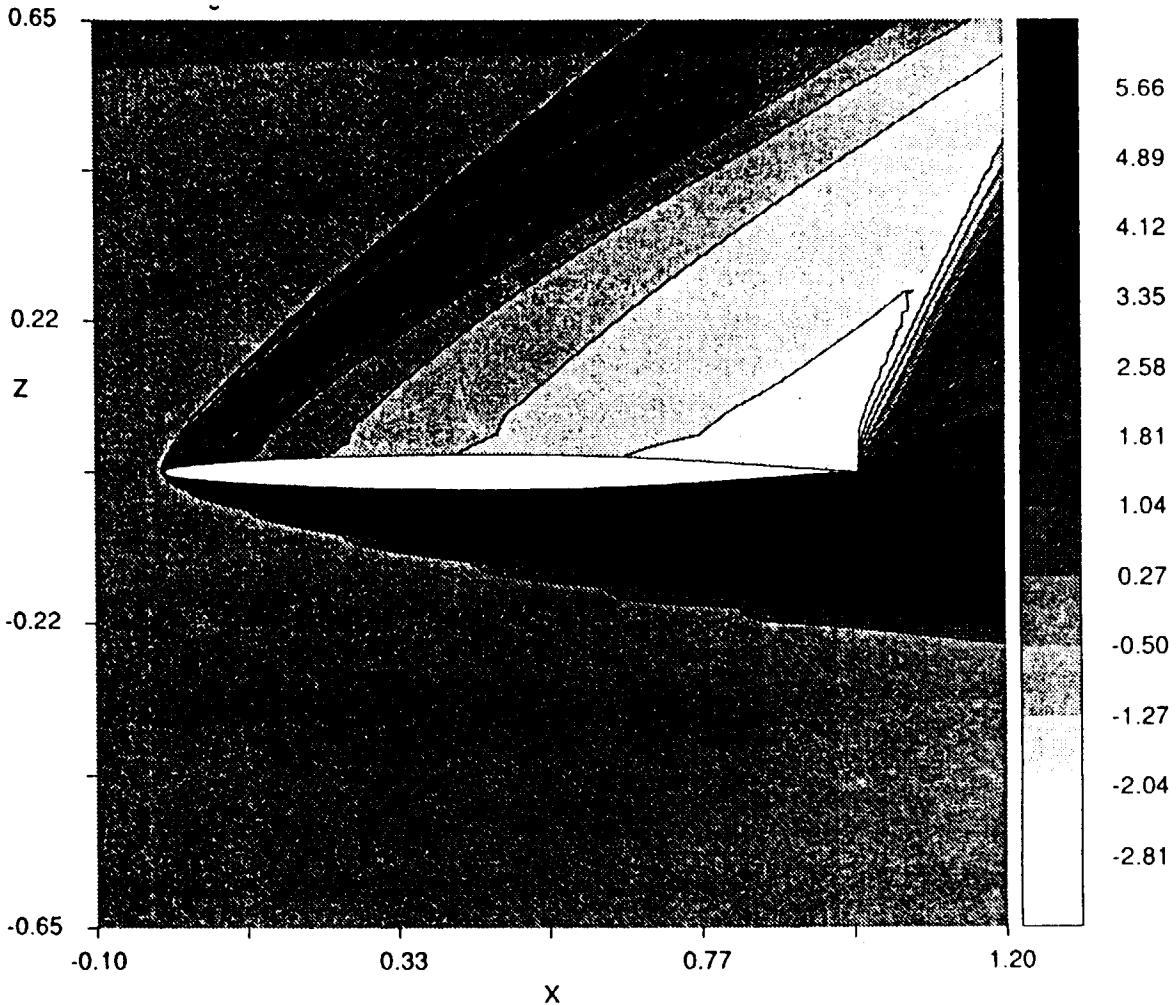

Figure 12b: TEAM Flowfield Results, Natural Log of Static Pressure Ratio: M = 23.0, α = 30°, δ = 0°, Inviscid Perfect Gas

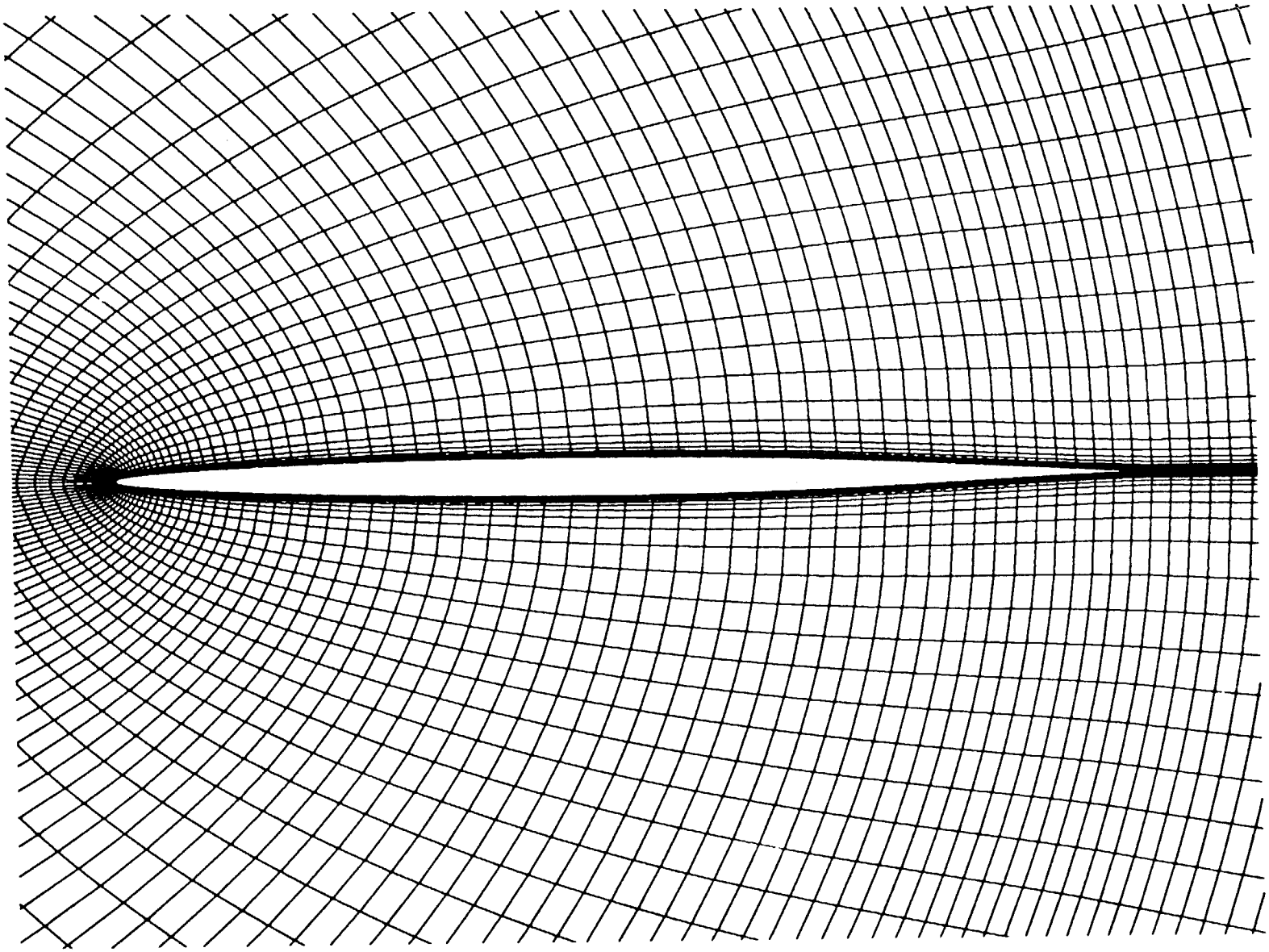

Figure 13: The TEAM Code Viscous Grid

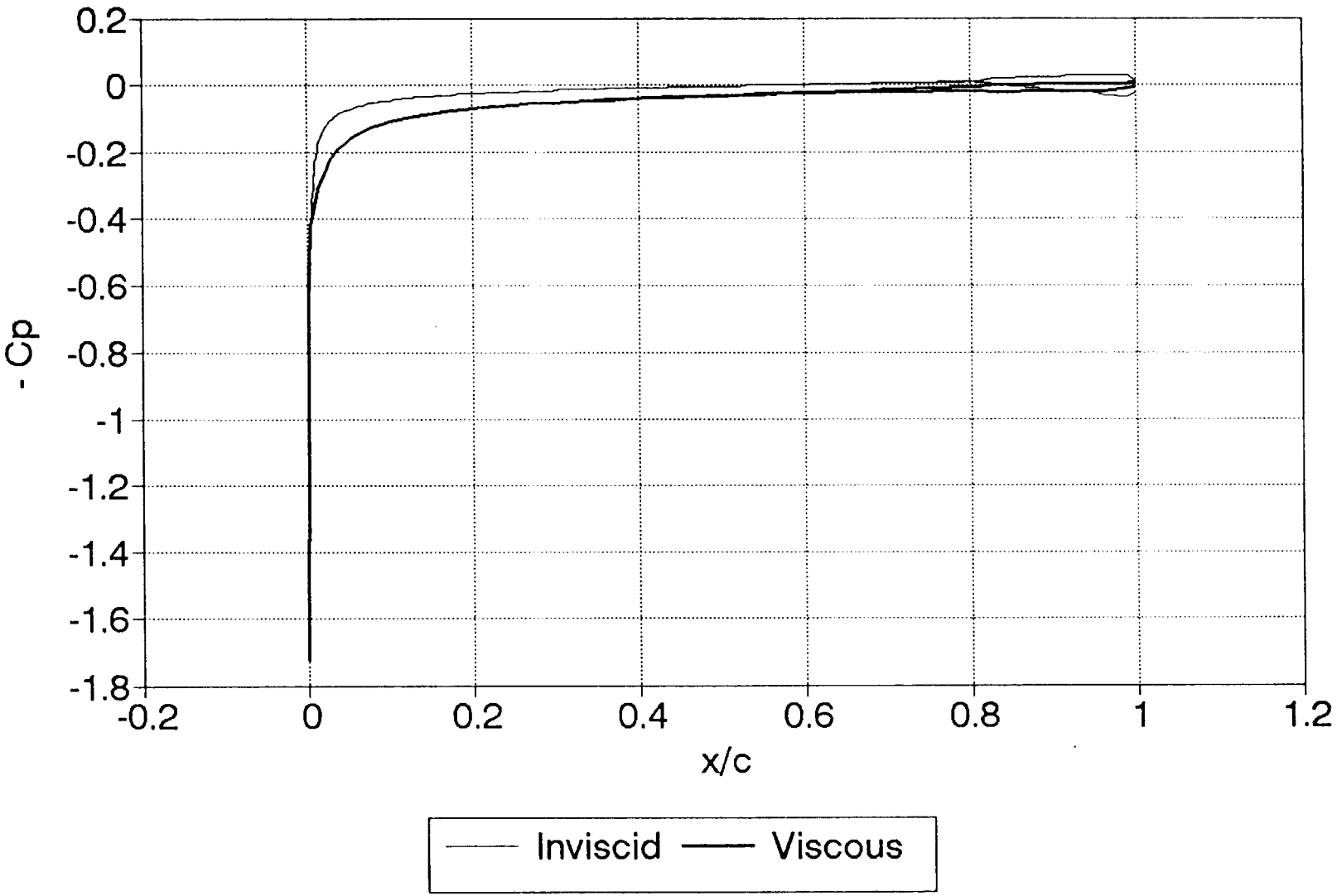

Figure 14: Comparison of Inviscid and Viscous TEAM Results: M = 6.83, α = 0°, δ = 10°, Perfect Gas

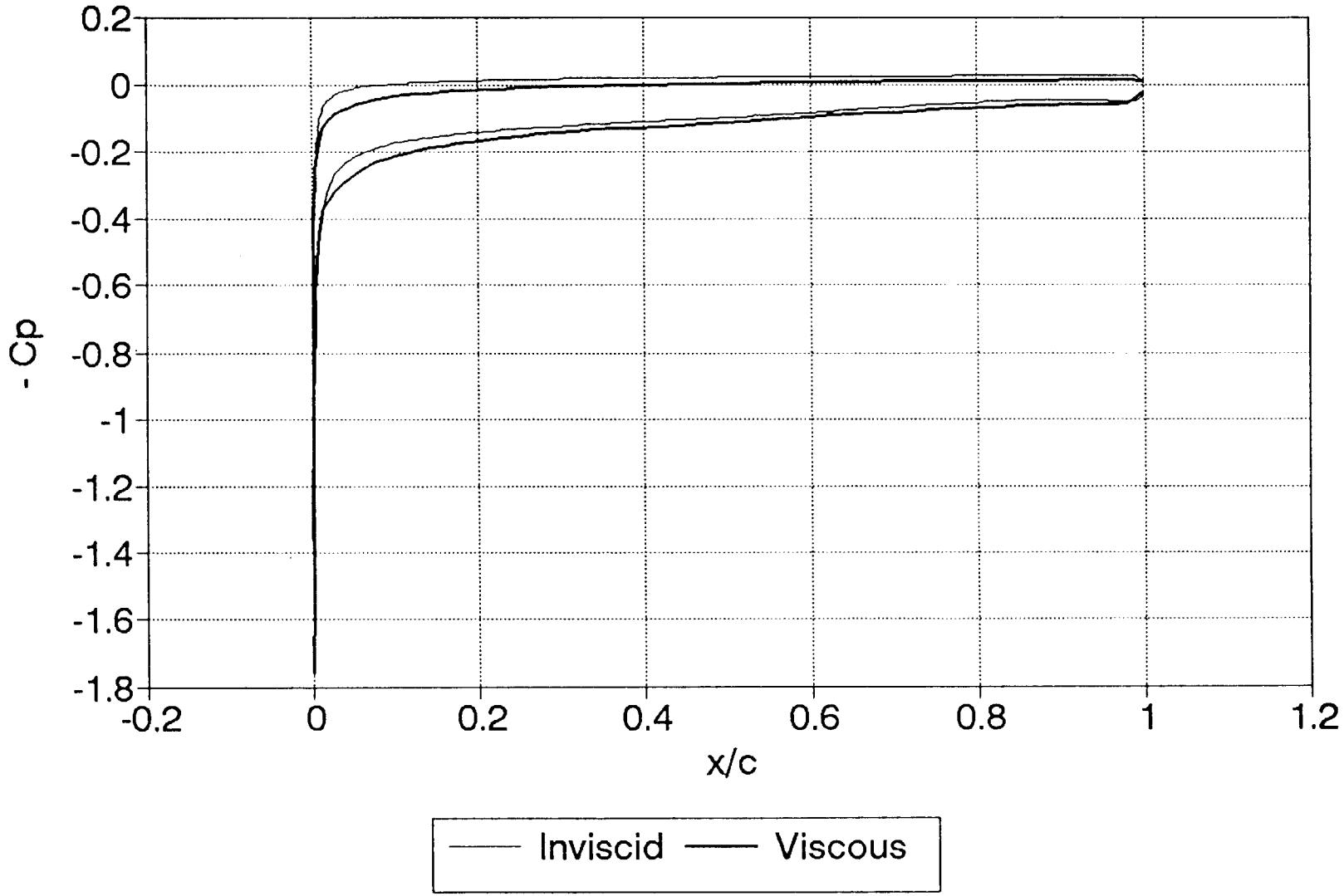

Figure 15: Comparison of Inviscid and Viscous TEAM Results: M = 6.83, α = 10°, δ = 0°, Perfect Gas

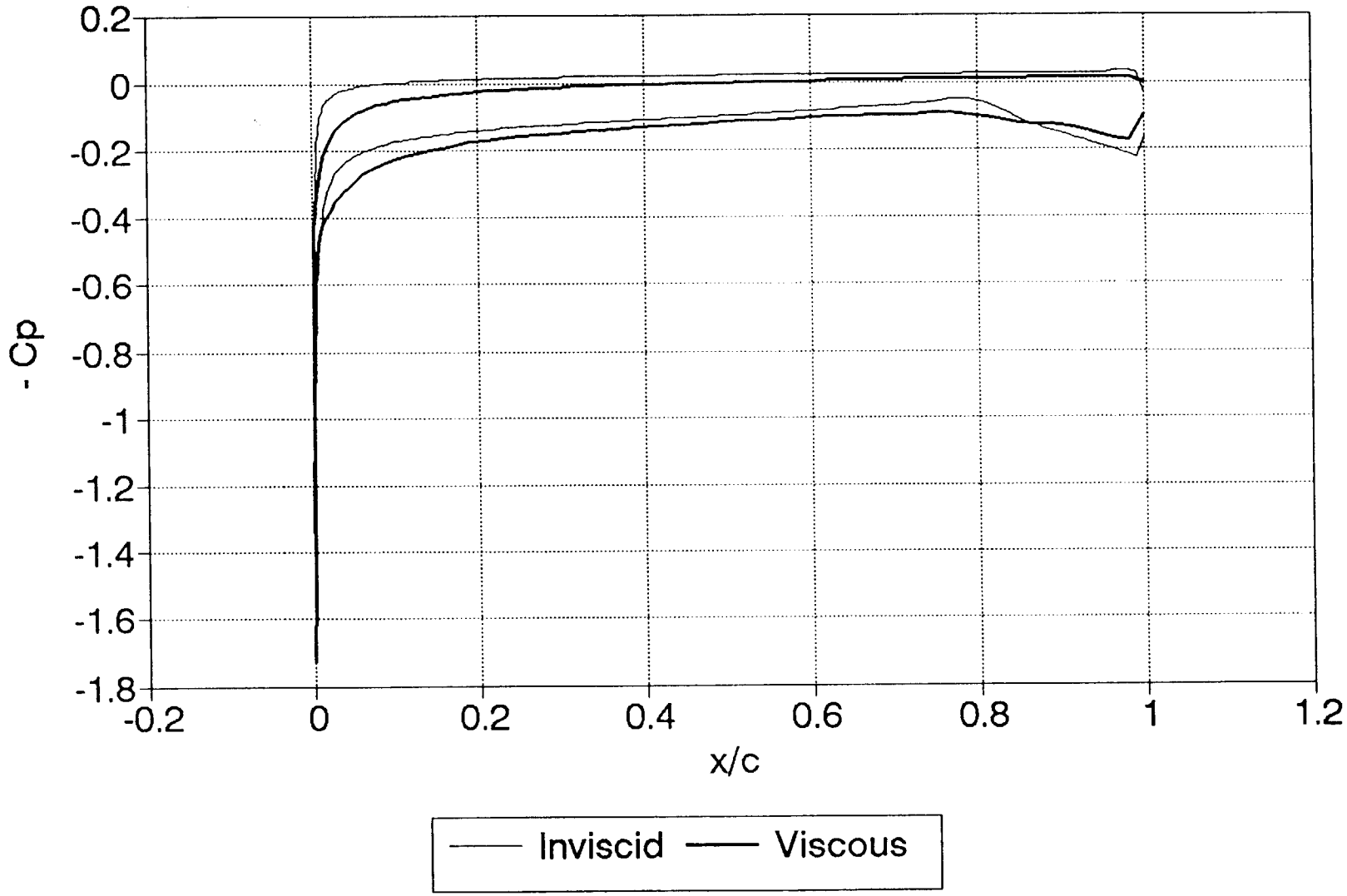

Figure 16: Comparison of Inviscid and Viscous TEAM Results: M = 6.83, α = 10°, δ = 10°, Perfect Gas

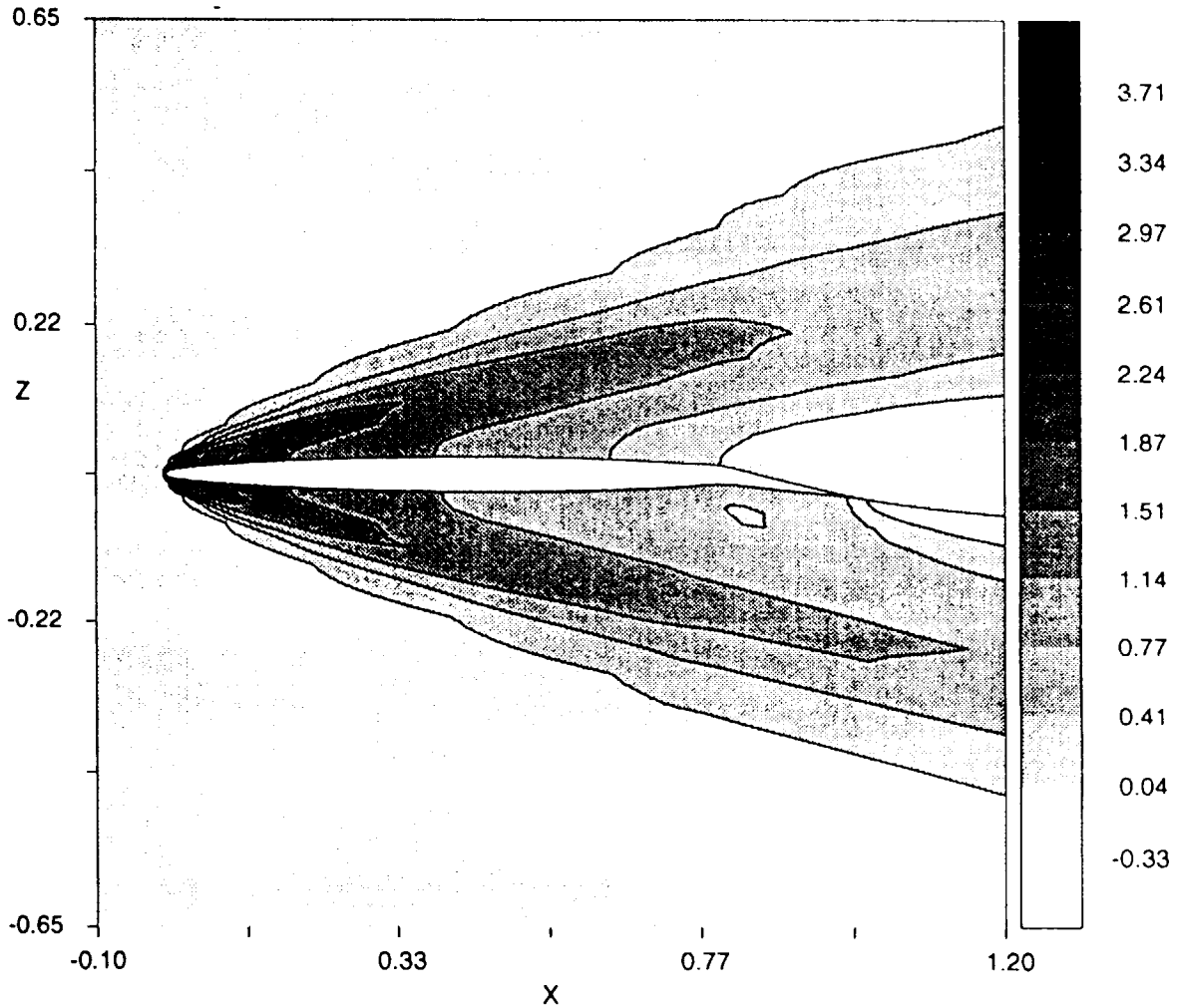

Figure 17: TEAM Flowfield Results, Natural Log of Static Pressure Ratio: M = 6.83, α = 0°, δ = 10°, Viscous Perfect Gas

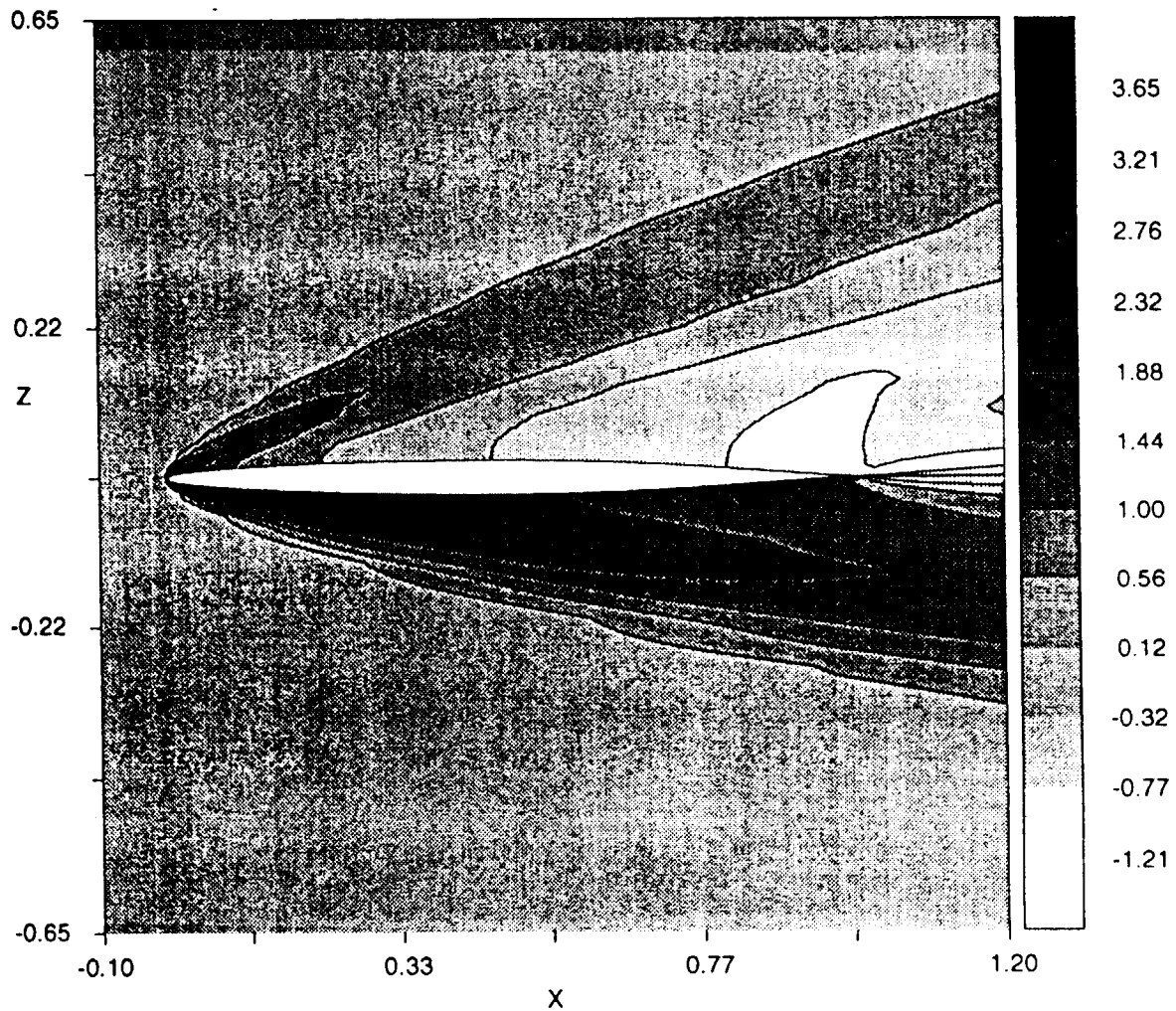

Figure 18: TEAM Flowfield Results, Natural Log of Static Pressure Ratio: M = 6.83, α = 10°, δ = 0°, Viscous Perfect Gas

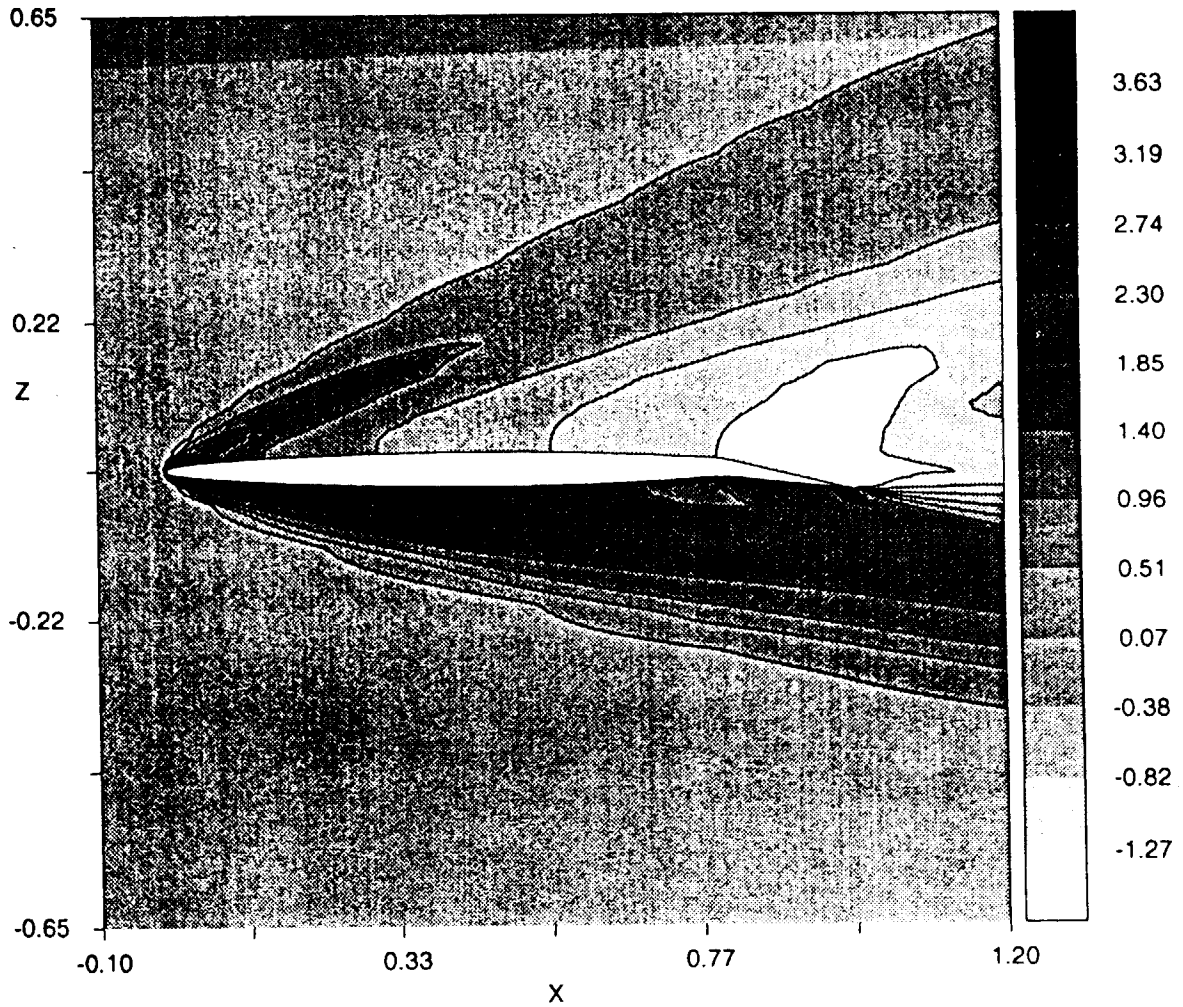

Figure 19: TEAM Flowfield Results, Natural Log of Static Pressure Ratio: M = 6.83, α = 10°, δ = 10°, Viscous Perfect Gas

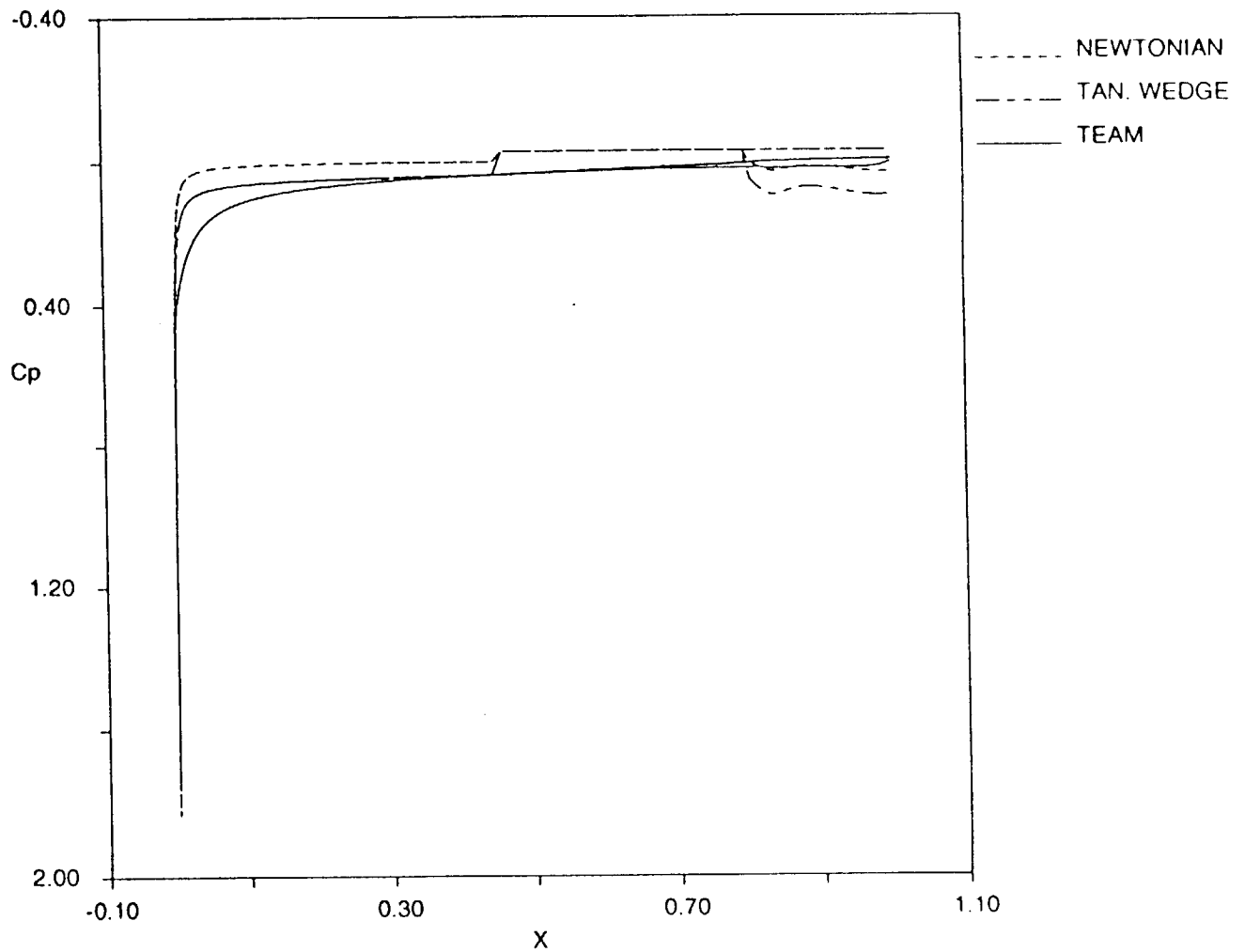

Figure 20: Coefficient of Pressure on the Surface: M = 6.83, α = 0°, δ = 10°, Viscous Perfect Gas

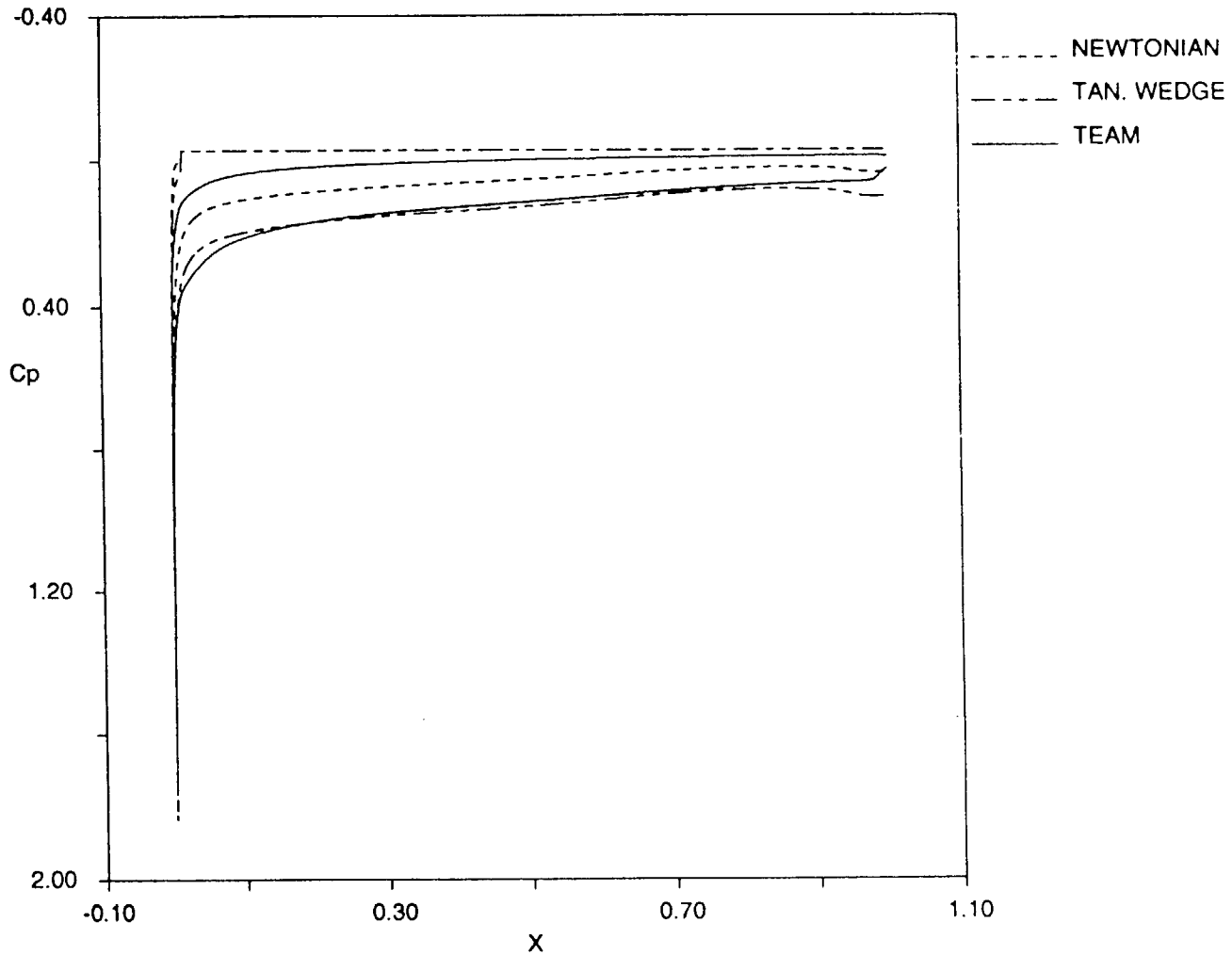

Figure 21: Coefficient of Pressure on the Surface: M = 6.83, α = 10°, δ = 0°, Viscous Perfect Gas

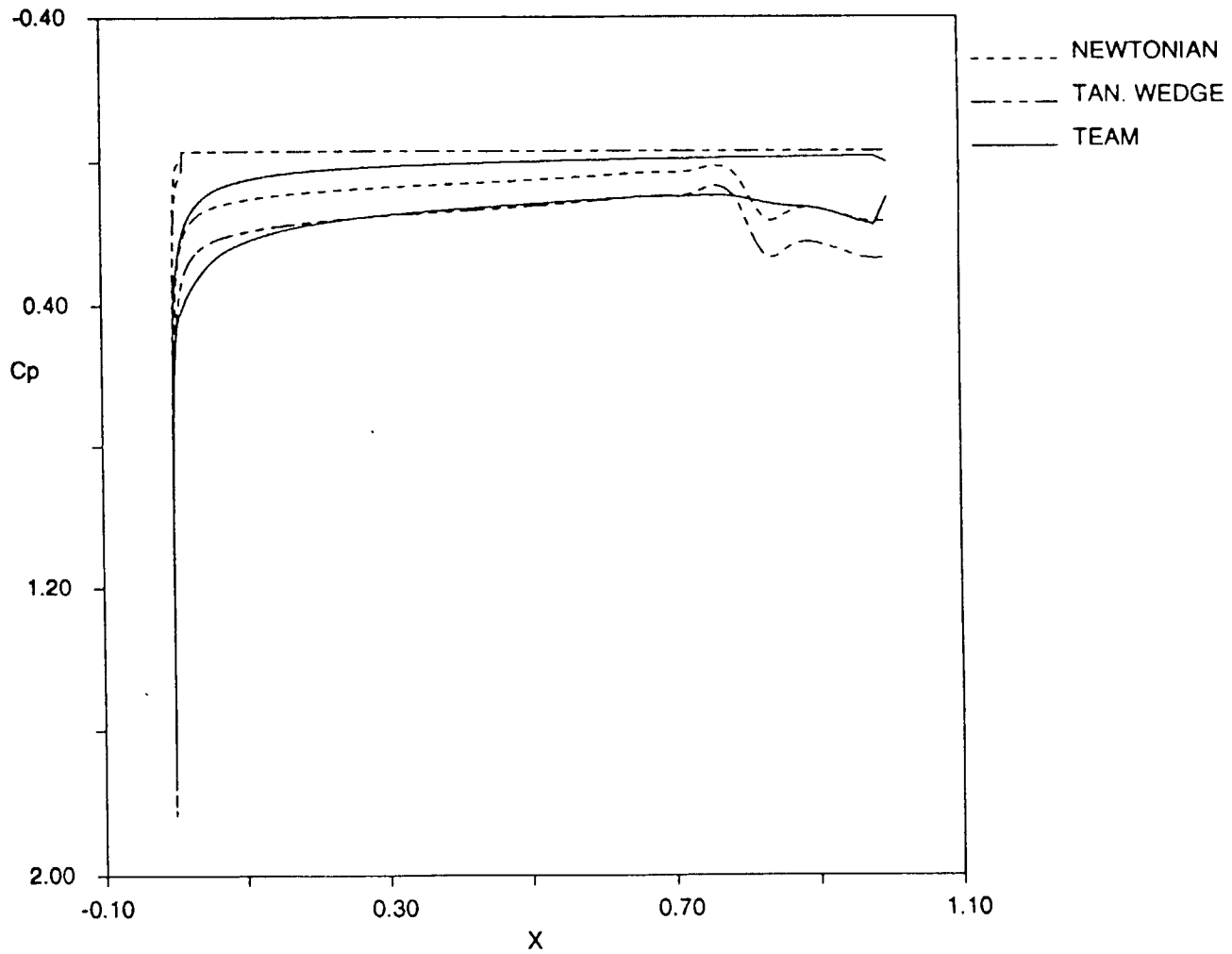

Figure 22: Coefficient of Pressure on the Surface: M = 6.83, α = 10°, δ = 10°, Viscous Perfect Gas

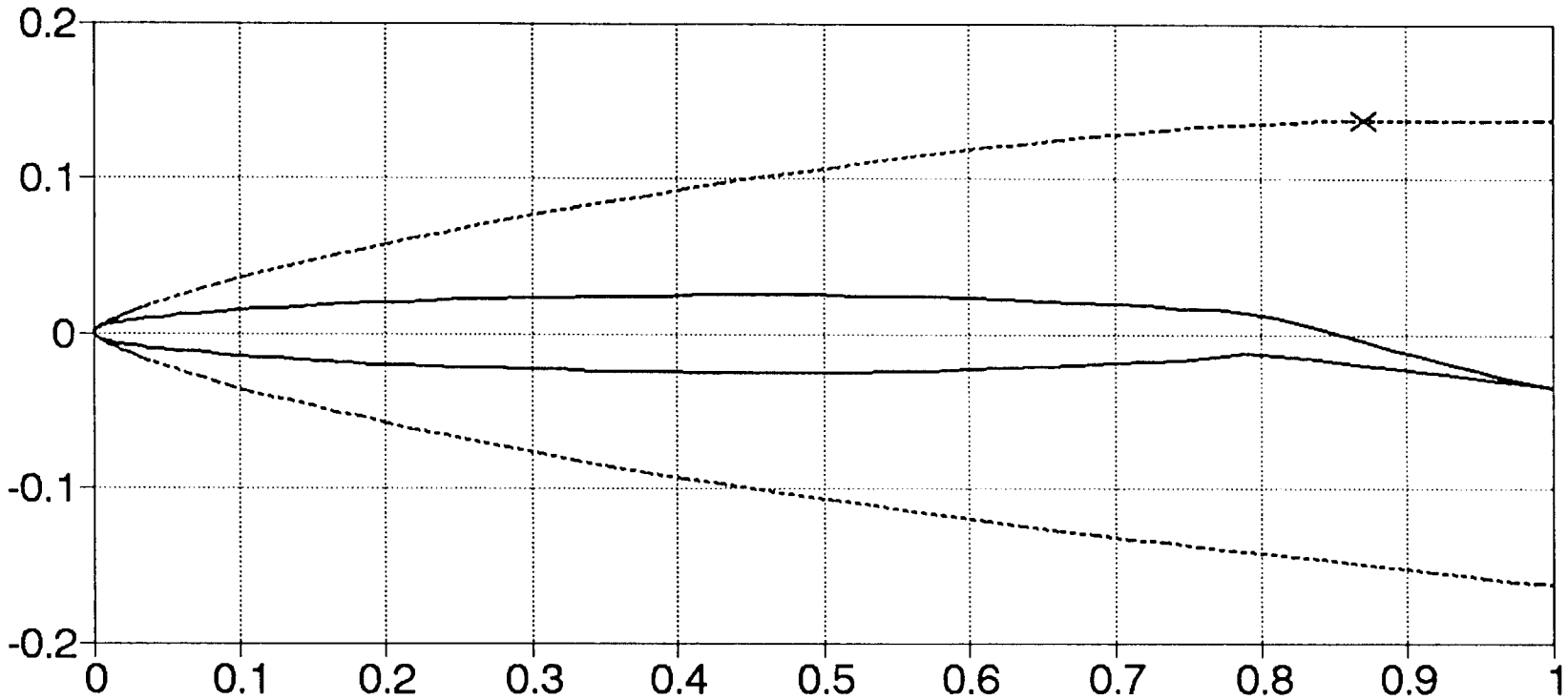

Figure 23: The X-15 Airfoil and its Shock-Layer: M = 6.83, α = 0°, δ = 10°, Viscous Perfect Gas (The 'X' on the upper surface indicates the initial point of hypersonic shielding.)

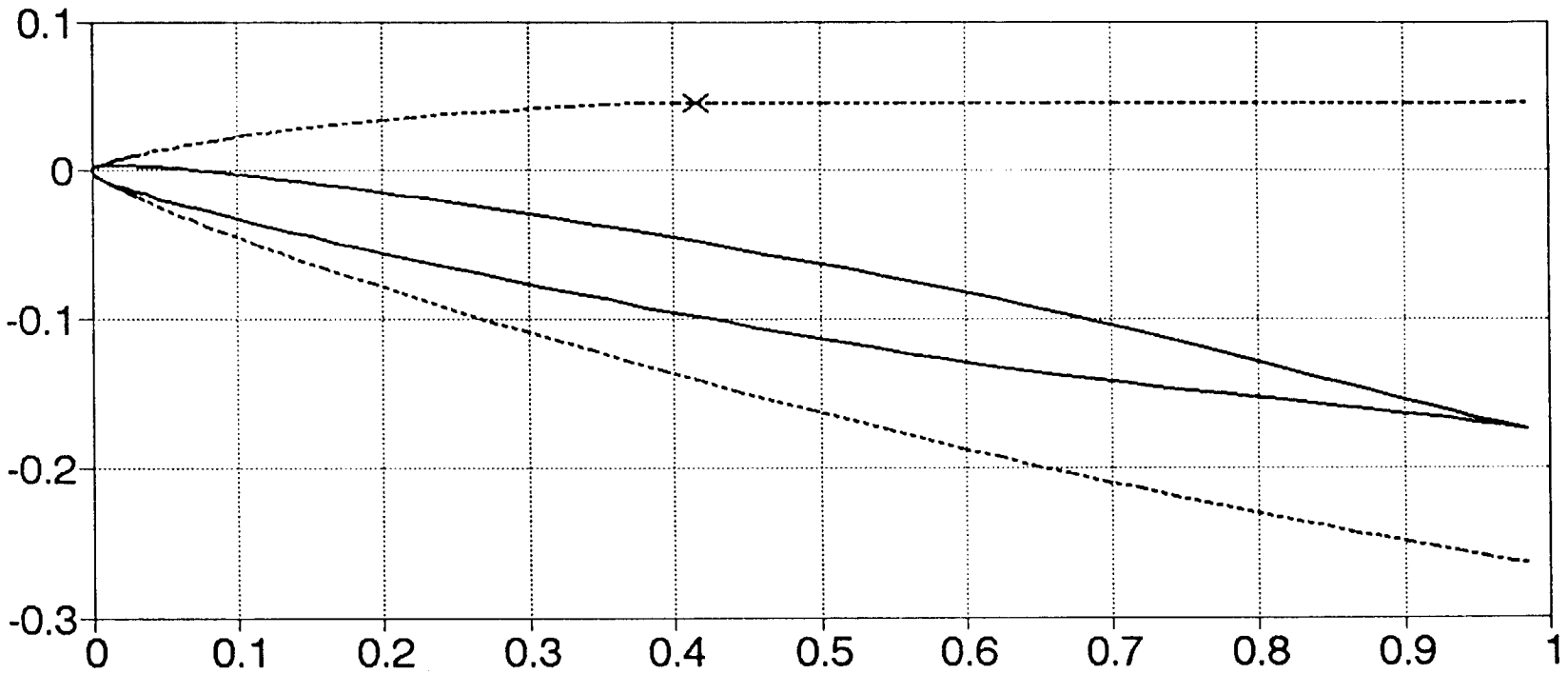

Figure 24: The X-15 Airfoil and its Shock-Layer: M = 6.83, α = 10°, δ = 0°, Viscous Perfect Gas (The 'X' on the upper surface indicates the initial point of hypersonic shielding.)

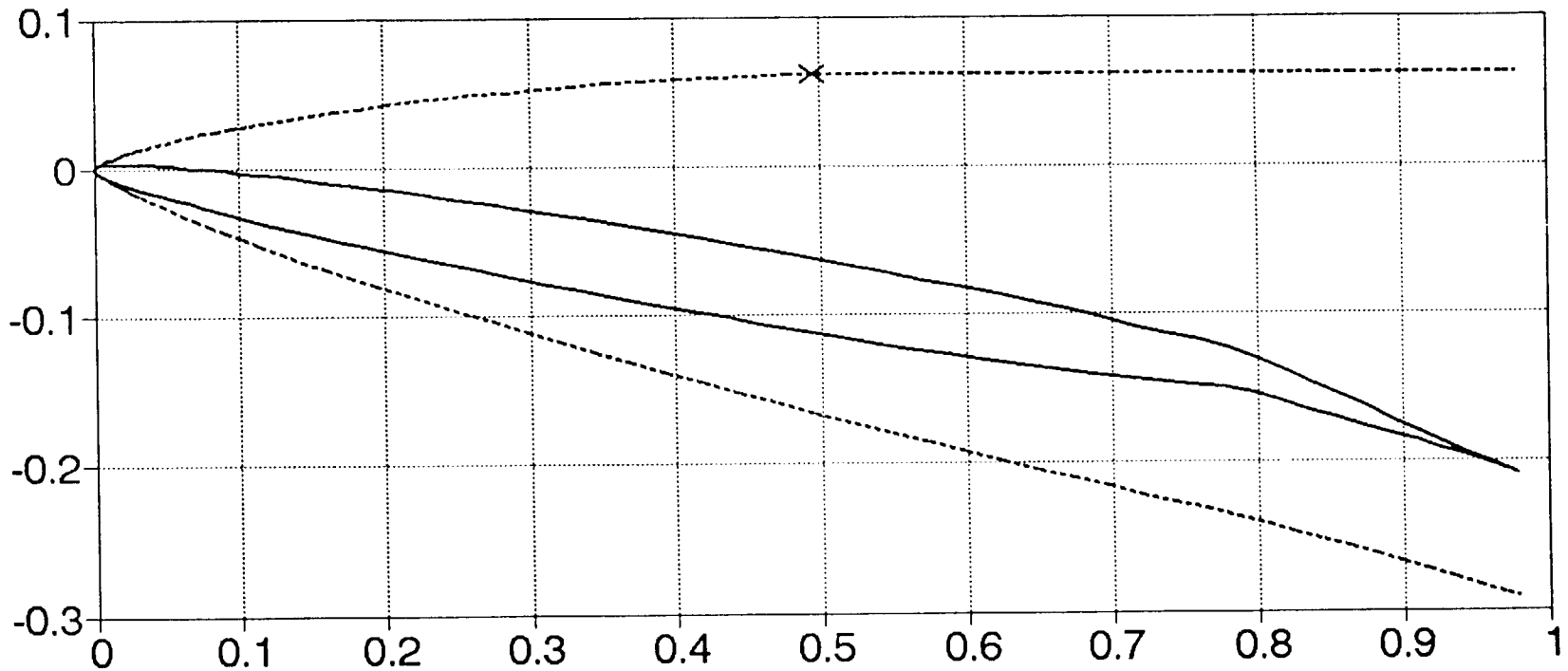

Figure 25: The X-15 Airfoil and its Shock-Layer: M = 6.83, α = 10°, δ = 10°, Viscous Perfect Gas (The 'X' on the upper surface indicates the initial point of hypersonic shielding.)

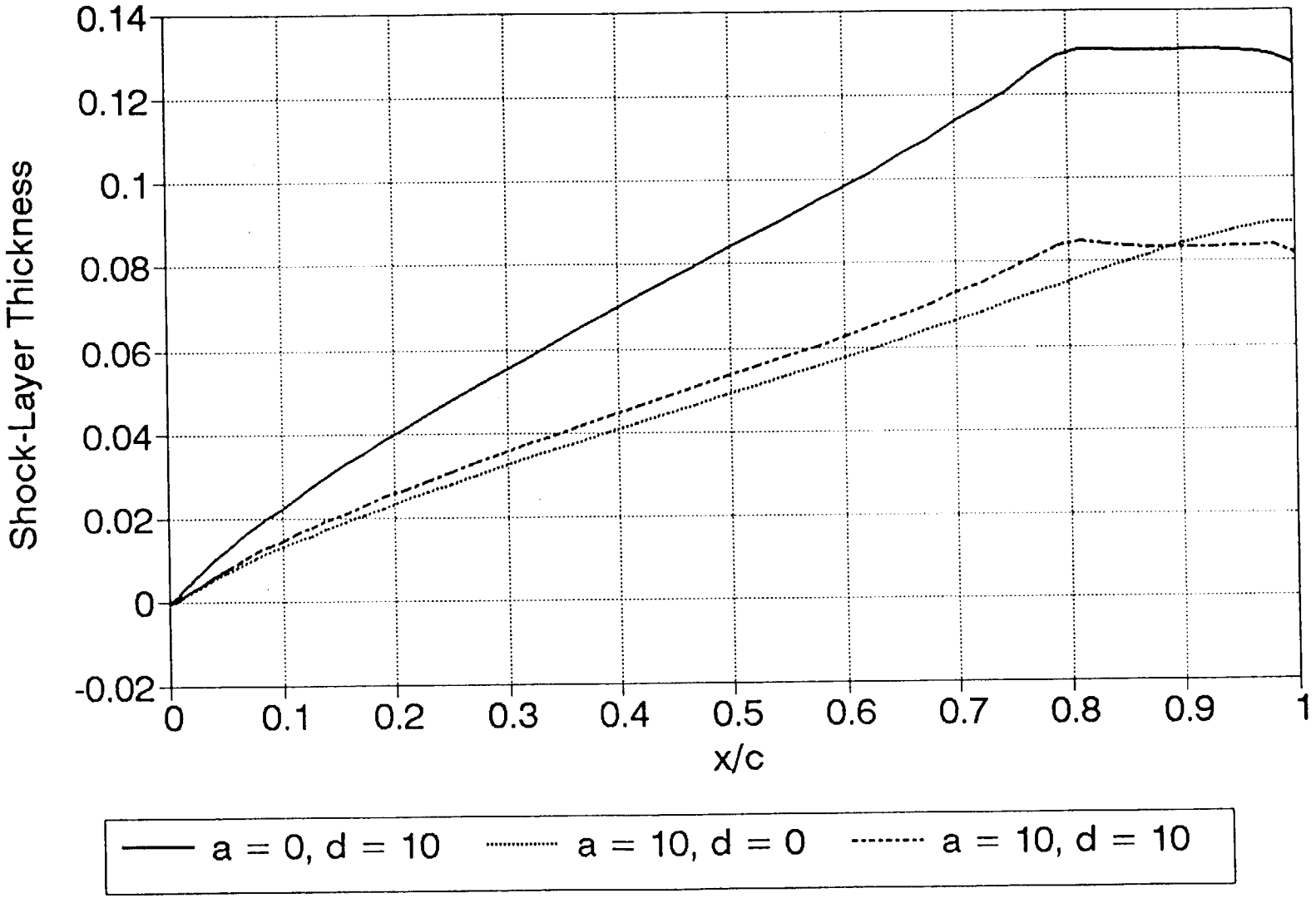

Figure 26: The Shock-Layer Thickness on the Lower Surface: M = 6.83, Viscous Perfect Gas

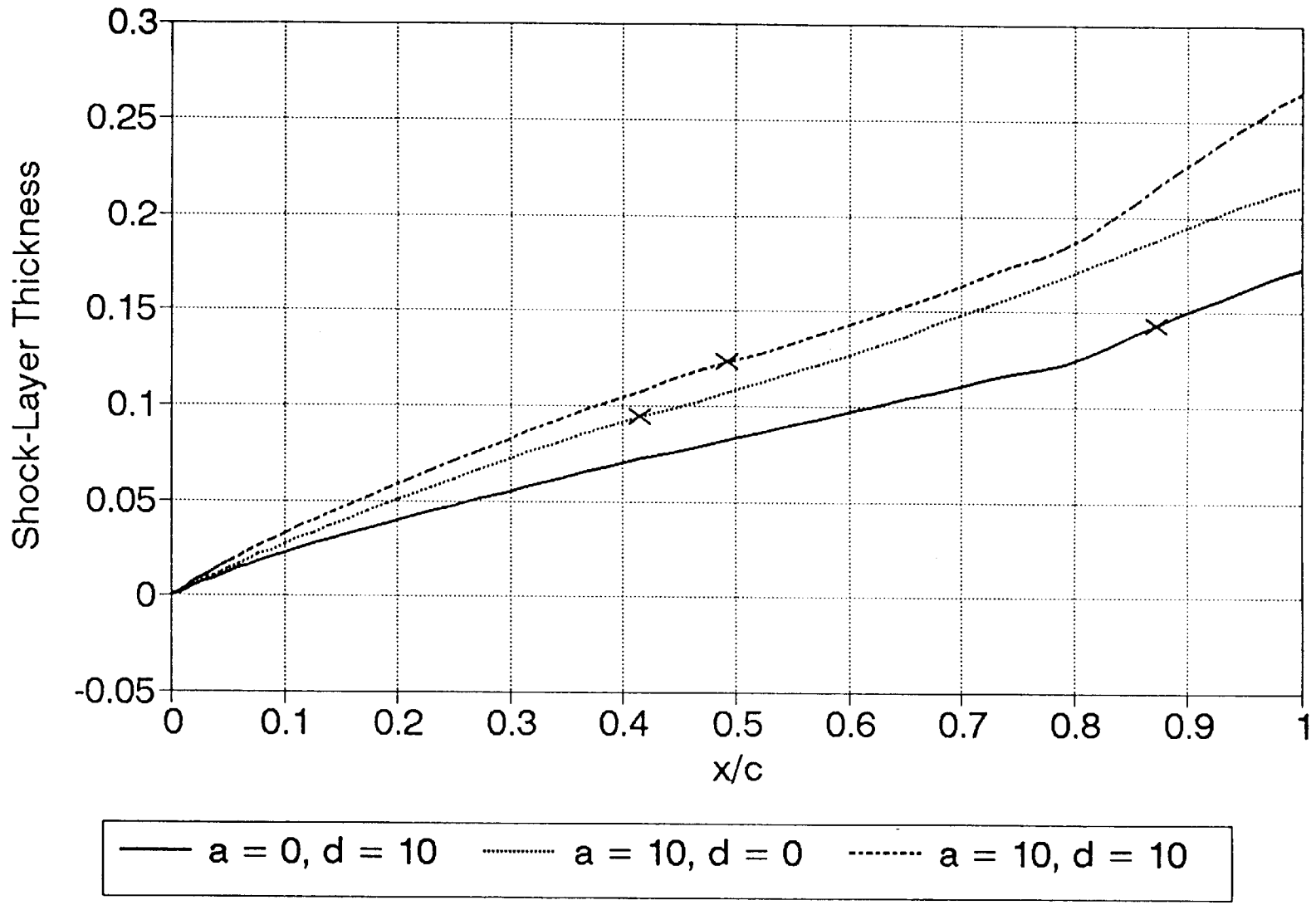

Figure 27: The Shock-Layer Thickness on the Upper Surface: M = 6.83, Viscous Perfect Gas (The X's indicate the initial points of hypersonic shielding.)